

On a new and homogeneous metallicity scale for Galactic classical Cepheids

I. Physical parameters ^{★, ★★}

B. Proxauf¹, R. da Silva^{2,3}, V.V. Kovtyukh^{4,5}, G. Bono^{1,2}, L. Inno⁶, B. Lemasse⁷, J. Pritchard²³, N. Przybilla⁸, J. Storm⁹, M.A. Urbaneja⁸, E. Valenti²³, M. Bergemann⁶, R. Buonanno^{1,10}, V. D’Orazi^{11,12}, M. Fabrizio^{2,3}, I. Ferraro², G. Fiorentino¹³, P. François^{14,15}, G. Iannicola², C.D. Laney^{16,17}, R.-P. Kudritzki^{18,19,20}, N. Matsunaga²¹, M. Nonino²², F. Primas²³, M. Romaniello²³, and F. Thévenin²⁴

¹ Dipartimento di Fisica, Università degli Studi di Roma Tor Vergata, via della Ricerca Scientifica 1, 00133 Rome, Italy
e-mail: giuseppe.bono@roma2.infn.it

² INAF-Osservatorio Astronomico di Roma, via Frascati 33, 00078 Monte Porzio Catone, Rome, Italy

³ Agenzia Spaziale Italiana, via del Politecnico snc, 00133 Rome, Italy

⁴ Astronomical Observatory, Odessa National University, Shevchenko Park, 65014 Odessa, Ukraine

⁵ Isaac Newton Institute of Chile, Odessa Branch, Shevchenko Park, 65014 Odessa, Ukraine

⁶ Max-Planck Institute for Astronomy, D-69117, Heidelberg, Germany

⁷ Astronomisches Rechen-Institut, Zentrum für Astronomie der Universität Heidelberg, Mönchhofstr. 12-14, 69120 Heidelberg, Germany

⁸ Institute for Astro- and Particle Physics, University of Innsbruck, Technikerstr. 25/8, 6020 Innsbruck, Austria

⁹ Leibniz-Institut für Astrophysik Potsdam, An der Sternwarte 16, 14482 Potsdam, Germany

¹⁰ INAF-Osservatorio Astronomico di Teramo, via Mentore Maggini snc, 64100 Teramo, Italy

¹¹ INAF-Osservatorio Astronomico di Padova, vicolo dell’Osservatorio 5, 35122, Padova, Italy

¹² Monash Centre for Astrophysics, School of Physics and Astronomy, Monash University, Melbourne, VIC 3800, Australia

¹³ INAF-Osservatorio Astronomico di Bologna, via Ranzani 1, 40127 Bologna, Italy

¹⁴ GEPI, Observatoire de Paris, CNRS, Université Paris Diderot, Place Jules Janssen, 92190 Meudon, France

¹⁵ UPJV, Université de Picardie Jules Verne, 33 rue St. Leu, 80080 Amiens, France

¹⁶ Department of Physics and Astronomy, N283 ESC, Brigham Young University, Provo, UT 84601, USA

¹⁷ South African Astronomical Observatory, PO Box 9, Observatory 7935, South Africa

¹⁸ Institute for Astronomy, University of Hawaii, 2680 Woodlawn Drive, Honolulu, HI 96822, USA

¹⁹ Max-Planck-Institute for Astrophysics, Karl-Schwarzschild-Str.1, 85741 Garching, Germany

²⁰ University Observatory Munich, Scheinerstr. 1, 81679 Munich, Germany

²¹ Department of Astronomy, School of Science, The University of Tokyo, 7-3-1 Hongo, Bunkyo-ku, Tokyo 113-0033, Japan

²² INAF-Osservatorio Astronomico di Trieste, via G. B. Tiepolo 11, 34143 Trieste, Italy

²³ European Southern Observatory, Karl-Schwarzschild-Str. 2, 85748 Garching bei München, Germany

²⁴ Laboratoire Lagrange, CNRS/UMR 7293, Observatoire de la Côte d’Azur, Bd de l’Observatoire, CS 34229, 06304 Nice, France

May 3, 2018

ABSTRACT

We gathered more than 1130 high-resolution optical spectra for more than 250 Galactic classical Cepheids. The spectra were collected with different optical spectrographs: UVES at VLT, HARPS at 3.6m, FEROS at 2.2m MPG/ESO, and STELLA. To improve the effective temperature estimates, we present more than 150 new line depth ratio (LDR) calibrations that together with similar calibrations already available in the literature allowed us to cover a broad range in wavelength ($5348 \leq \lambda \leq 8427 \text{ Å}$) and in effective temperatures ($3500 \leq T_{\text{eff}} \leq 7700 \text{ K}$). This means the unique opportunity to cover both the hottest and coolest phases along the Cepheid pulsation cycle and to limit the intrinsic error on individual measurements at the level of $\sim 100 \text{ K}$. Thanks to the high signal-to-noise ratio of individual spectra we identified and measured hundreds of neutral and ionized lines of heavy elements, and in turn, have the opportunity to trace the variation of both surface gravity and microturbulent velocity along the pulsation cycle. The accuracy of the physical parameters and the number of Fe I (more than one hundred) and Fe II (more than ten) lines measured allowed us to estimate mean iron abundances with a precision better than 0.1 dex. Here we focus on 14 calibrating Cepheids for which the current spectra cover either the entire or a significant portion of the pulsation cycle. The current estimates of the variation of the physical parameters along the pulsation cycle and of the iron abundances agree quite well with similar estimates available in the literature. Independent homogeneous estimates of both physical parameters and metal abundances based on different approaches that can constrain possible systematics are highly encouraged.

Key words. Galaxy: disk – stars: abundances – stars: fundamental parameters – stars: variables: Cepheids – stars: oscillations –

1. Introduction

Radially variable stars played a crucial role in the transition from qualitative to quantitative astrophysics. The reasons are manifold. They are simultaneously excellent primary distance indicators and very robust stellar tracers. The most popular ones are: *i*) RR Lyrae: old ($t > 10$ Gyr), low-mass stars; *ii*) Mira: intermediate-age (from a few hundred Myr to several Gyr) stars; and *iii*) classical Cepheids: young (from tens of Myr to a few hundred Myr) stars. Pulsation and evolutionary observables have been adopted for more than one century to constrain Galactic stellar populations (Baade 1958), and in particular to improve our knowledge of the physical mechanisms driving their pulsation properties and evolution (Kraft 1957; Preston 1964; Preston et al. 1965; Wallerstein 1972, 1979).

In this context, classical Cepheids (CCs) have been the cross-road of a paramount theoretical (Bono et al. 1999a,b; Fiorentino et al. 2007; Marconi et al. 2005; Anderson et al. 2016) and observational (Riess et al. 2016; Freedman & Madore 2010; Gieren et al. 2013; Pietrzynski et al. 2013; Soszynski et al. 2017) effort. They are the most popular primary distance indicators used to calibrate secondary indicators, and to estimate the Hubble constant. They are bright ($-2 \leq M_V \leq -7$ mag), and recent photometric investigations based on ground-based and/or space facilities provide accurate mean magnitudes for Cepheids located in external galaxies in the Local Group and in the Local Volume (Bono et al. 2010; Macri et al. 2015; Hoffmann et al. 2016, and references therein).

However, the spectroscopic investigations are lagging, and indeed they have been mainly focussed on Galactic Cepheids (Luck et al. 2011; Luck & Lambert 2011; Wallerstein et al. 2015; Genovali et al. 2014, 2015; Lemasle et al. 2013; da Silva et al. 2016, and references therein) and on a few nearby stellar systems like the Magellanic Clouds (Luck et al. 1998; Romaniello et al. 2008; Lemasle et al. 2017). CCs are also excellent physics laboratories, and indeed they have been used to investigate their dynamical properties along the pulsation cycle. They have been investigated both in the optical (Struve 1944; Kraft 1956) and in the near-infrared (NIR) regime (Sasselov et al. 1989; Sasselov & Lester 1990b). More recently, they have also been studied by Nardetto et al. (2009) to constrain the variation of the projection factor, in a very exhaustive paper by Wallerstein et al. (2015), and in the validation of the quasi-static approximation by Vasilyev et al. (2017a,b).

The elemental abundances are in a positive status since we are approaching an almost complete spectroscopic census of the currently known Galactic Cepheids (~450) based on high-resolution and high signal-to-noise (S/N) optical spectra (Bono et al., in prep.). Our group has been involved in a long-term project (DYONISOS) aimed at providing a homogeneous metallicity scale for field and cluster Galactic and Magellanic Cepheids. The current analyses mainly rely on the classical quasi-static approximation, in which the spectra of a CC, randomly collected along the pulsation cycle, are approximated with the physical properties of a static star with similar effective temperature, surface gravity and microturbulent velocity.

One of the key problems in dealing with spectroscopy of variable stars in the Cepheid instability strip is that the effective temperature, when moving from minimum to maximum light, changes by roughly 1 000 K. At the same time, the surface gravity also changes by up to 0.8–0.9 dex. These variations are correlated with the luminosity amplitude. The quasi-static approximation becomes more severe in dealing with spectra collected across pulsation phases affected by non-linear phenomena (formation and propagation of shocks), i.e., the phases along the rising branch or just before maximum compression. The reader is referred to Bono et al. (2000b) for a detailed discussion concerning these phenomena and their interplay with the Hertzsprung progression.

The effective temperature of CCs can be estimated using color-temperature relations, but this approach requires very accurate optical and NIR photometry. Moreover, this approach is prone to possible systematics introduced by reddening uncertainties and/or metallicity dependence. A very promising independent approach has been recently provided by Kervella et al. (2004) and Mérand et al. (2015) using optical and NIR interferometric measurements of the diameter of nearby CCs. The same applies to the infrared surface brightness (IRSB) method by Storm et al. (2011a,b) and by Groenewegen (2008) using optical/NIR photometry and radial velocities to constrain the angular diameter variations.

In this context, a temperature diagnostic that appears quite robust is the Line Depth Ratio (LDR). It relies on plain physical assumptions: the depth ratio of several pairs of absorption lines is strongly correlated with the effective temperature. To minimize the dependence of the abundance on the surface gravity and possible uncertainties in the continuum location, the lines forming these pairs should come from the same (or a similar) element, have similar wavelengths, be weak, non saturated, and come from neutral species (Gray 2005).

The use of the LDR method to estimate the effective temperature of CCs was pioneered by several authors: Sasselov & Lester (1990a), Krockenberger et al. (1998), Kovtyukh & Gorlova (2000, hereinafter KG00), and by Kovtyukh et al. (2003b, hereinafter K03). In particular, KG00 provided a set of calibrations based on 32 pairs of lines. K03 provided 105 new LDR calibrations using more than 180 FGK main sequence stars covering ~ 1 dex in iron abundance ($-0.5 \leq [\text{Fe}/\text{H}] \leq 0.5$) and for which were available high-resolution ($R \sim 42\,000$), high S/N spectra, together with accurate trigonometric parallaxes from HIPPARCOS and effective temperature estimates with an accuracy of the order of 1%. Subsequently, Kovtyukh (2007, hereinafter K07) obtained a set of 131 LDR calibrations using 161 FGK supergiants, increasing the valid range in temperature to about 3600–7800 K (F0 I–K5 I). The equivalent width (EW) measurements of each pair provide an independent estimate of the effective temperature. These LDRs have been quite successful, being used in many recent spectroscopic investigations of CCs (e.g. Andrievsky et al. 2002a,b; Lemasle et al. 2007, 2008; Genovali et al. 2013, 2014), with a typical precision of the order of 150 K.

The main aim of this investigation is to provide new and homogeneous estimates of the intrinsic parameters (effective temperature, surface gravity, microturbulent velocity) for CCs and to constrain their impact on the iron abundance. The key advantage of the current investigation when compared with similar analyses available in the literature is that we are dealing with 14 calibrating CCs covering a broad range in pulsation period ($0.53 \leq \log P \leq 1.62$) and in metal abundance ($-0.11 \leq [\text{Fe}/\text{H}] \leq 0.35$ dex). The current sample was defined as "calibrating" CCs, since the

* Partly based on observations made with ESO Telescopes at the La Silla/Paranal Observatories under program IDs: 072.D-0419, 073.D-0136 and 190.D-0237 for HARPS spectra; 084.B-0029, 087.A-9013, 074.D-0008, 075.D-0676 and 60.A-9120 for FEROS spectra; 081.D-0928, 082.D-0901, 089.D-0767 and 093.D-0816 for UVES spectra.

** Partly based on data obtained with the STELLA robotic observatory in Tenerife, an AIP facility jointly operated by AIP and IAC.

Table 1. Calibrating Cepheids, for which high-resolution spectra cover either a substantial fraction or the entire pulsation cycle.

Name	$R_G^a \pm \sigma$ [pc]	α_{ICRS}	δ_{ICRS}	Period ^b [days]	$T_0^b - 2400\,000$ [days]	[Fe/H] ^a lit $\pm \sigma$	N_F	N_H	N_U	N_S	N_{tot}
V340 Ara	4657 ± 427	16:45:19.112	-51:20:33.393	20.80876	44881.2740	0.33 ± 0.09	26	...	6	...	32
η Aql	7750 ± 452	19:52:28.368	+01:00:20.370	7.17679	43368.8611	0.14 ± 0.02	11	11
S Cru	7593 ± 451	12:54:21.998	-58:25:50.214	4.68973	44301.5560	0.08 ± 0.10	1	12	13
β Dor	7936 ± 451	05:33:37.517	-62:29:23.369	9.84308	47913.0970	-0.06 ± 0.10	...	46	46
ζ Gem	8273 ± 452	07:04:06.531	+20:34:13.074	10.15072	50139.4010	-0.11 ± 0.10	...	47	...	81	128
Y Oph	7141 ± 452	17:52:38.702	-06:08:36.870	17.12415	44083.4490	0.12 ± 0.04	...	8	8
RS Pup	8585 ± 444	08:13:04.216	-34:34:42.696	41.44002	53014.2808	0.21 ± 0.10	...	15	15
UZ Sct	5309 ± 448	18:31:22.368	-12:55:43.350	14.7482	45496.3631	0.33 ± 0.08	28	...	6	...	34
AV Sgr	5980 ± 454	18:04:48.780	-22:43:56.600	15.41153	53109.1989	0.35 ± 0.17	28	...	5	...	33
VY Sgr	5862 ± 453	18:12:04.568	-20:42:14.580	13.55845	50891.6007	0.33 ± 0.12	30	...	4	...	34
XX Sgr	6706 ± 453	18:24:44.501	-16:47:49.816	6.42414	44822.6740	-0.01 ± 0.06	5	...	5
Y Sgr	7483 ± 452	18:21:22.986	-18:51:36.002	5.77335	40762.4310	0.11 ± 0.03	...	20	...	3	23
R TrA	7519 ± 451	15:19:45.713	-66:29:45.742	3.38924	52365.1127	0.16 ± 0.11	1	14	15
RZ Vel	8249 ± 445	08:37:01.303	-44:06:52.848	20.39689	45003.4620	0.19 ± 0.10	1	11	12

Notes. From left to right the columns give name, galactocentric distance, right ascension, declination, pulsation period, and zero-phase reference epoch of maximum light in the V-band. Column seven lists the iron abundance available in the literature. The columns from eight to eleven show the number of optical spectra used for each spectrograph: N_F , FEROS; N_H , HARPS; N_U , UVES; N_S , STELLA. The last column lists the total number of spectra per target.

References. ^(a) Genovali et al. (2014); ^(b) This investigation.

optical high-resolution spectra cover the pulsation cycle either fully or for the most part. Indeed, the number of spectra per object range from five (XX Sgr) to more than one hundred (ζ Gem).

The structure of the paper is the following. In § 2 we present the entire spectroscopic dataset and we discuss the S/N and the wavelength range covered by the spectra. In § 3 we discuss the different strategies adopted to pre-reduce and to calibrate the spectra. Section 3.1 deals with the adopted linelists and with the approach adopted to measure the equivalent widths. In § 4 we discuss the determination of the atmospheric parameters and the radial velocities, including the LDR calibrations used to derive the effective temperature and their validity range. The determination of the iron abundances is presented in § 5, together with the variations along the pulsation cycle. The summary of the results and the future perspective of this project are given in § 6.

2. Spectroscopic datasets

The spectroscopic datasets partly analyzed in the current paper, and that will be used for a new series of papers, are spectra collected at three different telescopes of the *European Southern Observatory* (ESO): the *Ultraviolet and Visual Echelle Spectrograph* (UVES, Dekker et al. 2000) at the VLT, the *High Accuracy Radial velocity Planet Searcher* (HARPS, Mayor et al. 2003) at the 3.6m, and the *Fiber-fed Extended Range Optical Spectrograph* (FEROS, Kaufer et al. 1999) at the 2.2m MPG/ESO. A list of CCs was defined for the three spectrographs and the related spectra were downloaded from the ESO archive, forming the datasets UVES TS (for *This Study*, 32 spectra, 3 targets), HARPS (199 spectra, 9 targets), and FEROS TS (486 spectra, 169 targets).

The quoted spectra were complemented with spectra collected by Inno et al. (ID: 093.D-0816, dataset UVES IN, 154 spectra, 46 targets), Kovtyukh et al. (2016, dataset UVES KO, 9 spectra, 1 target, and dataset FEROS KO, 2 spectra, 2 targets), Genovali et al. (2015, dataset UVES GE, 120 spectra, 73 targets). We also included 134 high-resolution spectra for 5 targets collected with the STELLA Echelle Spectrograph (SES, Strassmeier et al. 2004, 2010). As a whole, we ended up with

1136 high-resolution spectra for 251 Cepheids, explicitly accounting for the multiplicity of objects among different spectrographs.

The spectral resolution of the quoted spectrographs for the instrument settings used are: $R \sim 40\,000$ (UVES), $R \sim 115\,000$ (HARPS), $R \sim 48\,000$ (FEROS), and $R \sim 55\,000$ (STELLA). The corresponding wavelength ranges for our sample are: *i*) UVES: ~ 3050 – 3870 Å; ~ 3760 – 4985 Å, ~ 5684 – 7520 Å, ~ 7663 – 9458 Å; ~ 4786 – 5750 Å, ~ 5833 – 6806 Å; ~ 4980 – 5952 Å, ~ 6035 – 7002 Å; ~ 6700 – 8523 Å, ~ 8659 – 10422 Å; *ii*) HARPS: ~ 3781 – 5304 Å, ~ 5337 – 6912 Å; *iii*) FEROS: ~ 4000 – 9216 Å; and *iv*) STELLA: ~ 3872 – 8813 Å.

The current spectroscopic dataset can be divided into three different subgroups:

Calibrating Cepheids:

a) Phase dependence – For 14 targets in our sample the spectra cover either a significant part or the entire pulsation cycle. This is the subsample of CCs that we analyze in the present paper and that we will adopt to constrain the accuracy of the intrinsic parameters and, in particular, their impact on the iron abundance. Note that the bulk of CCs are strictly periodic on long evolutionary time scales. This means that we take advantage of the strict periodicity in cyclic variations.

b) Cluster Cepheids – Our sample includes 14 CCs that are candidate cluster variables. The number of spectra per target ranges from one to more than one hundred. These targets will be adopted to link field and cluster CCs on the same metallicity scale.

Cepheids with new iron abundances: This subgroup includes roughly 50 Cepheids for which we secured high-resolution UVES spectra and for which no metallicity estimate is available in the literature. The number of spectra per target ranges from 1 to more than fifty.

Cepheids with homogeneous iron abundances: We derive homogeneous iron abundances based on high-resolution spectra for 216 CCs. The number of spectra per target ranges from 1 to almost fifty.

In the current investigation we focus on the 14 calibrating CCs with multi-epoch spectroscopic measurements. Details

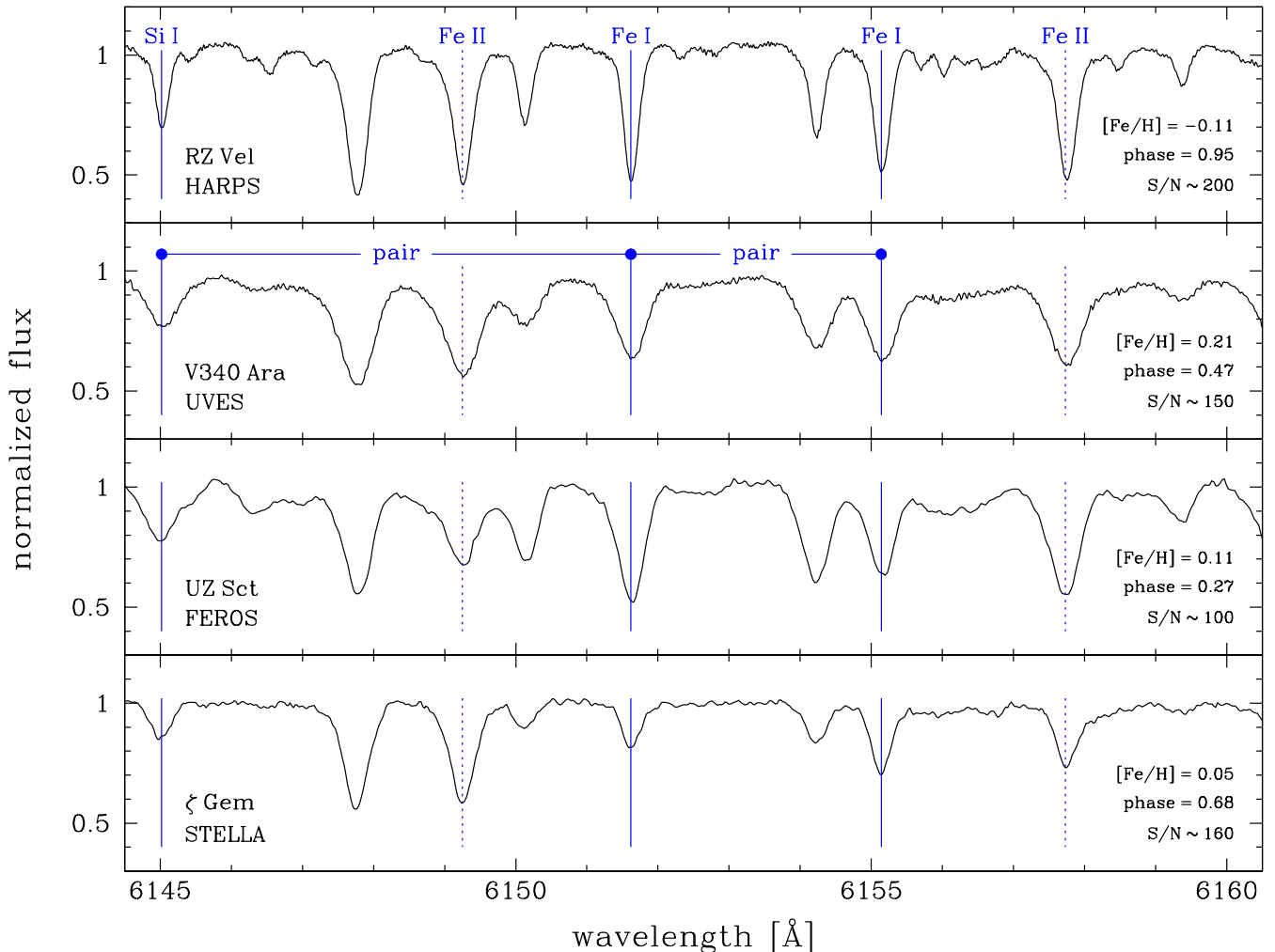


Fig. 1. Examples of high-resolution spectra for different calibrating classical Cepheids collected with different spectrographs: HARPS, UVES, FEROS, and STELLA. The vertical lines display the position either of iron lines only used for the metallicity determination (dashed) or of lines adopted also in the LDR method (solid). The name of the Cepheid, its mean metallicity, the phase, and the signal-to-noise ratio of these example spectra around 6000 Å are also labelled.

on the number of spectra are given in Table 1. The spectra of EV Sct and X Sgr were initially included in our analysis, but afterwards excluded. In a detailed spectroscopic investigation based on high-resolution spectra, Kovtyukh & Andrievsky (1999) found that EV Sct shows strong line asymmetries and even split lines. They suggested that this object might be a binary system with two short period Cepheids, in spite of the observed phase coherence. Concerning X Sgr, Mathias et al. (2006), on the basis of both optical and NIR high-resolution spectroscopy, found strong dynamical variations in the outermost layers. Moreover, optical and NIR interferometric data (Li Causi et al. 2013; Gallenne et al. 2014) showed evidence of a possible companion, which is also suggested by the orbital velocity curve determined by Feast et al. (2008). The interested reader is also referred to Szabados (1990, 2003); Evans (1992); Groenewegen (2008) for a more detailed discussion. These two CCs were also included in the list of candidate non-radial pulsators by Kovtyukh et al. (2003a).

3. Data reduction and analysis

The spectra have to be prepared for the later analysis by doing an initial pre-reduction (up to the wavelength calibration step). The spectra from UVES and HARPS (phase-3) were already pre-reduced by their own pipeline. FEROS spectra were reduced with a modified version of the FEROS-DRS pipeline developed by one of us (J. Pritchard). Several FEROS spectra taken before 2004 could not be reduced due to a change in the CCD software architecture from the BIAS controller to FIERA and therefore a different file structure. The current FEROS sample includes 355 spectra, with the remaining 133 not yet included in the analysis.

The next step, the continuum normalization, was required for UVES (except UVES GE, already continuum-normalized), HARPS and FEROS. Before the normalization, UVES and HARPS spectra were split into blue and red spectral parts due to the big central gap present therein. The continuum normalization was performed using the *Image Reduction and Analysis Facility* (IRAF¹) by fitting cubic spline functions to a set of continuum windows visually selected in the spectra. For UVES and

¹ Distributed by the National Optical Astronomy Observatories (NOAO), USA.

Table 2. Mean parameters derived for the calibrating Cepheids.

Name	$\langle T_{\text{eff}} \rangle \pm \sigma$ [K]	$\langle \log g \rangle \pm \sigma$	$\langle v_r \rangle \pm \sigma$ [km s $^{-1}$]	[Fe I/H] $\pm \sigma$	[Fe II/H] $\pm \sigma$	[Fe/H] $\pm \sigma$ (std)	N_{spec}
V340 Ara	5293 \pm 42	1.14 \pm 0.11	4.77 \pm 0.19	0.24 \pm 0.07	0.22 \pm 0.05	0.23 \pm 0.04 (0.07)	7
η Aql	5479 \pm 39	1.11 \pm 0.09	3.43 \pm 0.15	0.26 \pm 0.05	0.23 \pm 0.03	0.24 \pm 0.03 (0.09)	11
S Cru	6014 \pm 21	1.64 \pm 0.08	3.08 \pm 0.14	0.09 \pm 0.03	0.08 \pm 0.04	0.09 \pm 0.03 (0.04)	13
β Dor	5557 \pm 13	1.35 \pm 0.04	3.78 \pm 0.07	-0.04 \pm 0.02	-0.02 \pm 0.02	-0.03 \pm 0.01 (0.05)	46
ζ Gem	5494 \pm 7	1.12 \pm 0.03	3.22 \pm 0.04	0.15 \pm 0.01	0.17 \pm 0.01	0.16 \pm 0.01 (0.05)	128
Y Oph	5612 \pm 33	0.99 \pm 0.11	3.22 \pm 0.18	0.06 \pm 0.05	0.09 \pm 0.06	0.08 \pm 0.04 (0.05)	8
RS Pup	5381 \pm 27	0.84 \pm 0.08	4.66 \pm 0.13	0.13 \pm 0.04	0.15 \pm 0.03	0.14 \pm 0.02 (0.07)	14
UZ Sct	5038 \pm 36	1.24 \pm 0.11	4.86 \pm 0.18	0.13 \pm 0.07	0.07 \pm 0.09	0.11 \pm 0.05 (0.09)	8
AV Sgr	5228 \pm 38	1.18 \pm 0.11	4.86 \pm 0.18	0.25 \pm 0.07	0.32 \pm 0.03	0.31 \pm 0.02 (0.08)	8
VY Sgr	5340 \pm 35	0.98 \pm 0.09	4.59 \pm 0.16	0.21 \pm 0.06	0.27 \pm 0.04	0.25 \pm 0.03 (0.08)	10
XX Sgr	5843 \pm 41	1.30 \pm 0.13	2.98 \pm 0.22	0.09 \pm 0.06	0.03 \pm 0.06	0.06 \pm 0.04 (0.02)	5
Y Sgr	5924 \pm 26	1.75 \pm 0.06	4.11 \pm 0.11	0.07 \pm 0.03	-0.02 \pm 0.02	0.00 \pm 0.01 (0.06)	22
R TrA	6039 \pm 25	1.97 \pm 0.08	4.01 \pm 0.13	0.02 \pm 0.03	-0.04 \pm 0.03	-0.01 \pm 0.02 (0.03)	15
RZ Vel	5479 \pm 29	1.23 \pm 0.09	4.62 \pm 0.14	0.09 \pm 0.04	0.08 \pm 0.04	0.08 \pm 0.03 (0.06)	12

Notes. From left to right the columns give name, effective temperature, surface gravity, microturbulent velocity, iron abundances, and number of spectra used to compute the mean values. These are the weighted mean and its uncertainty computed from the values in Table 4. The standard deviation of the mean computed using individual abundances of both Fe I and Fe II is also shown.

HARPS spectra we normally used 1st order functions, but for FEROS spectra high-order (20-50) cubic spline functions were required given their large wavelength range.

The radial velocity of the objects was determined using IRAF by cross-correlating the target spectrum with an observed solar template spectrum in the rest frame (Solar Flux Atlas, Kurucz et al. 1984) degraded to the UVES resolution. The UVES GE spectra were already in the rest frame and served as templates. For FEROS spectra, because of possible contamination due to bleeding during the wavelength calibration (Fran ois et al. 2006), we preferred to adopt the radial velocities derived by the routine used to measure the EWs (see Sect. 3.1). For STELLA spectra, the radial velocities come directly from the STELLA reduction pipeline (Weber et al. 2012), which is based on IRAF. It performs the standard data reduction steps including scattered light removal and continuum normalization. The radial velocities are based on cross-correlation with a synthetic template spectrum. In the case of Cepheids a G-type star template is used. The resulting radial velocities have estimated uncertainties of about 0.2 km s $^{-1}$.

The spectra were examined for EW measurements by checking the S/N in different continuum regions in the spectra. From the preliminary S/N estimates derived from these blocks in combination with a visual check, the different spectra were classified as low, intermediate, or high-quality exposures, and the usability for further analysis, especially the metallicity determination, was evaluated. The UVES GE sample has already been marked with sufficient S/N by the original authors. The UVES KO and UVES IN S/N ratios could be taken directly from the ESO archive. For FEROS the S/N ratios range from 25 to 475, for HARPS they are between 145 and 400, and for UVES TS they cover a range between 235 and 480. We noticed that many of the FEROS spectra have been classified as low-quality exposures, and have then not been included in the metallicity and effective temperature determination. Examples of HARPS, UVES, FEROS, and STELLA spectra of different metallicities and with different S/N estimates (measured around 6000 Å) are depicted in Fig. 1.

3.1. Equivalent width measurements

The equivalent widths were measured using the *Automatic Routine for line Equivalent widths in stellar Spectra* (ARES, Sousa et al. 2007, 2015). First, a global set of common input parameters was used, and then the parameters were individually adjusted, giving better fits of the spectral line profiles. As mentioned in Sect. 3, ARES also performs an automatic estimate of the radial velocity, whose values were used in the case of FEROS spectra.

Three linelists were created:

a) one built by combining four individual linelists received from Kovtyukh and used to derive the effective temperature (T_{eff}) of the objects (153 lines);

b) one from Genovali et al. (2013), complemented with the *Gaia-ESO Survey* (GES, Gilmore et al. 2012; Randich et al. 2013), and cross-checked with the *Vienna Atomic Line Database* (VALD3, Ryabchikova et al. 2015), containing iron features (615 lines);

c) one from Genovali et al. (2015) and da Silva et al. (2016) including lines belonging to other elements (113 lines, α -, s- and r-elements).

The atomic lines used for effective temperature determination are listed in Table 3. The linelist of the other elements will be discussed in a forthcoming paper.

4. Atmospheric parameters

4.1. New and old LDR calibrations

Although being widely used, the LDRs by KG00 are based on polynomial relations hampered by a limited range in effective temperature (4700-6700 K) and in wavelength (5670-6850 Å). The former limitation affects the accuracy when dealing with spectra collected across the hottest pulsation phases, the latter one when dealing with spectra having higher S/N in redder wavelengths ($\lambda > 6500$ Å). For this reason, K07 extended the number of calibrations to a total of 131 pairs of lines located in the wavelength range between 5348 and 6768 Å. The key advantage of

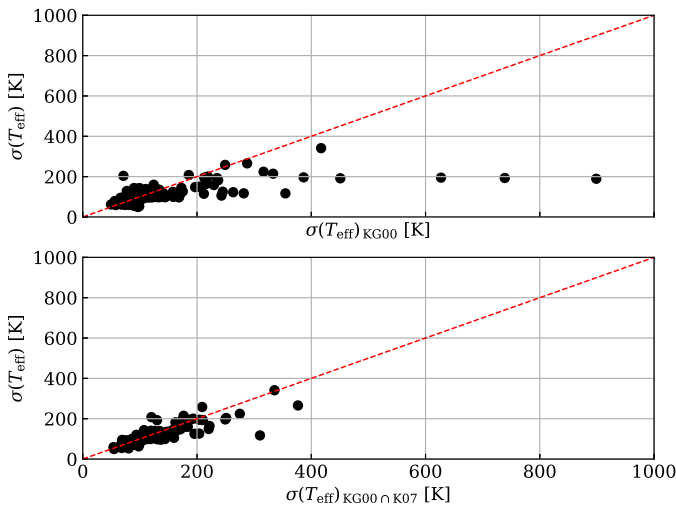


Fig. 2. Standard deviations of the effective temperature estimates for the 199 HARPS spectra. *Top panel*: the entire set of 257 LDR calibrations used in the current investigation ($\text{KG00} \cap \text{K07} \cap \text{K17}$) is compared with the 32 calibrations provided by KG00. *Bottom panel*: the same as in the top panel, but the comparison is between this study and the calibrations provided by KG00 \cap K07.

the new LDRs is that they allow effective temperature estimates up to 7800 K.

To further improve the range in wavelength covered by the LDR calibrations, one of us (V. Kovtyukh) identified 151 new pairs of lines. Here we publish these new calibrations, which are based on effective temperatures estimated by K07. They fixed the temperature scale using non-variable supergiants for which the effective temperature was already available in the literature using independent approaches. Subsequently, they applied the new temperature scale to classical Cepheids and they only retained the LDRs for which the standard deviation was smaller than 110 K.

In case the same pair appears in different calibrations, we always selected the most recent one. All in all we ended up with 257 pairs of lines ranging from 5348 to 8427 Å, and covering the temperature range from 3500 to 7700 K. To our knowledge this is the most complete list of LDRs ever compiled for F-K spectral type stars. Moreover, as shown in Fig. 2, the standard deviations of the effective temperature determinations are clearly reduced with the increasing number of calibrations. The figure shows the results for the HARPS sample, but it is also valid for the other samples.

We are dealing therefore with three different sets of LDR calibrations:

- a) KG00: 32 calibrations;
- b) K07: discussed 131 calibrations, but the analytical functions are presented here for the first time;
- c) K17 (this investigation): 151 new calibrations.

From the 257 calibrations (multiplicity removed), based on 153 lines, 257 independent estimates of the effective temperature could be obtained. The list of the analytical relations for the LDRs used in this investigation is given in Table 3.

4.2. Effective temperature estimation

Several calibrations were removed, since they provide effective temperatures significantly different from the bulk of the LDRs. Such outliers in the temperature distribution may be caused ei-

ther by blends in the specific pair or by limited S/N. Each calibration also has a certain range of validity where the LDR can be used. For many of our sample stars we did not have a previous estimate of their effective temperature, therefore, we performed an iterative process. In each iteration, the calibrations had to pass a sigma clipping and were then accepted only if a defined interval around the median temperature was overlapping with the temperature range of the calibration. The clippings were stopped when no more calibrations were cut.

Once the clippings were finished, the mean and median temperature was computed from the remaining values. The number of calibrations that survived the sigma clipping was typically quite high (~ 100) so that a solid statistical basis was present and the standard deviations were relatively low (< 100 K) for most of the spectra.

We performed a number of numerical simulations assuming no sigma clipping and we found that the mean/median values are minimally affected, while the standard deviation increases to ~ 150 K. The approach we adopted to estimate the effective temperature for the individual spectra can be summarized as follows:

- a) Take all available LDR calibrations and calculate individual effective temperatures.
- b) Calculate the effective temperature mean/median/ σ .
- c) If the effective temperature of a given LDR calibration is out of 2σ from the median and $\sigma > 100$ K, discard the LDR; if no LDR calibration is discarded go to (d), otherwise go back to (b).
- d) Check if the median value is within the validity range of the calibrations; discard all the LDR calibrations that do not cover the derived median; if no LDR calibration is discarded go to (e), otherwise go back to (b).
- e) Calculate the final mean/median/ σ .

The median values of effective temperatures and the standard deviations, together with other parameters, derived for individual spectra of the calibrating Cepheids are listed in Table 4. Spectra for which the effective temperature could not be estimated, as explained in Sect. 3, are listed in Table 5.

In order to validate the effective temperature estimates based on the new sets of LDRs, we performed a detailed comparison with similar estimates available in the literature. The top panel of Fig. 3 shows the comparison between the current effective temperature amplitude ($\Delta T_{\text{eff}} = T_{\text{eff}}^{\text{max}} - T_{\text{eff}}^{\text{min}}$) and similar estimates for 60 Galactic Cepheids for which Storm et al. (2011a, hereinafter S11) applied the IRSB method to estimate individual distances and intrinsic parameters. We estimated the ΔT_{eff} by fitting the effective temperature curves with sinusoidal functions. Cepheids for which the phase coverage is not optimal (Y Oph, UZ Sct, AV Sgr, and XX Sgr) were marked with black crosses. The vertical error bars display the standard deviations on the fitted functions. Typical error bars on the ΔT_{eff} values from S11 are smaller than the symbol size. Data plotted in this panel display the typical V-shape distribution (Bono et al. 2000a), i.e., pulsation amplitudes display a well defined minimum across the so-called Hertzsprung progression ($\log P \sim 1.0$, Bono et al. 2000b). The agreement between the two data sets is quite good in the period range in common.

We also compared the current ΔT_{eff} estimates with similar evaluations provided by Pel (1978) using multi-band Walraven photometry (bottom panel of Fig. 3). Note that CCs identified by the author as having known or suspected companions, or having other peculiarities, were not included in the figure. The agreement is once again good over the entire period range in common. Note that this approach is only based on photometric measurements.

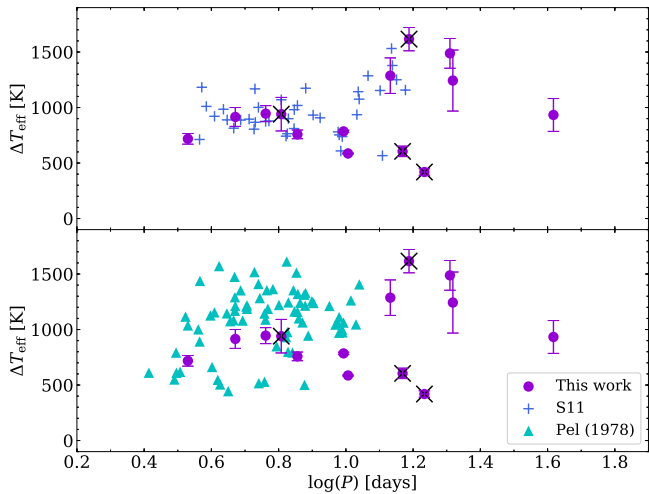


Fig. 3. Effective temperature amplitude ($\Delta T_{\text{eff}} = T_{\text{eff}}^{\text{max}} - T_{\text{eff}}^{\text{min}}$) as a function of the logarithmic period. The black crosses indicate stars for which the available spectra do not properly cover the maximum and minimum of the pulsation cycle.

4.3. Surface gravity and microturbulent velocity

The surface gravity ($\log g$) was derived through the ionization equilibrium between Fe I and Fe II lines, and the microturbulent velocity (v_t) was derived by minimizing the slope in the [Fe I] vs. EW plot. This means that the $\log g$ value is changed until the Fe I and Fe II lines provide the same abundance, within the errors, while the v_t value is changed until the dependence of the derived abundances on the EWs is removed. Indeed, weak and strong lines are supposed to provide the same elemental abundances. In the iterative procedure, the T_{eff} values (derived as described in Sect. 4.2) are kept fixed, and the $\log g$ and v_t values are changed until the aforementioned conditions are satisfied.

For the determination of these parameters, we used the MOOG LTE radiative code (Sneden 2002) applied to model atmospheres derived by interpolation in the grid of Castelli & Kurucz (2004). We did not perform a specific test to constrain the difference when using different grids of atmosphere models. However, recent detailed results available in the literature (Heiter & Eriksson 2006; Gustafsson et al. 2008) support a very good agreement in the spectral range (F-K) typical of classical Cepheids. The standard solar abundances adopted by the MOOG code (version of July 2014) come from Asplund et al. (2009). Though they have been recently revised by Grevesse et al. (2015) and by Scott et al. (2015b,a), we decided to use the abundances from Asplund et al. (2009) for consistency with our previous spectroscopic analyses.

Table 2 lists the weighted mean of the surface gravity and microturbulent velocity computed for the 14 calibrating Cepheids using the multiple values listed in Table 4. In that table, the uncertainties on the individual estimates of $\log g$ and v_t are not listed, but they are expected to be of the order of ~ 0.3 dex and $\sim 0.5 \text{ km s}^{-1}$, respectively (see Genovali et al. 2014). In Table 2, the uncertainty on the weighted mean is shown.

In the top panel of Fig. 4 we show the comparison among the current surface gravity amplitudes ($\Delta \log g$) and similar estimates by Pel (1978) and by S11. As in Fig. 3, stars from Pel (1978) with known or suspected companions, or having other peculiarities, were not included. The three different datasets agree quite well within the errors. Note that the two Cepheids with larger surface gravity amplitudes (UZ Sct and AV Sgr) are among those

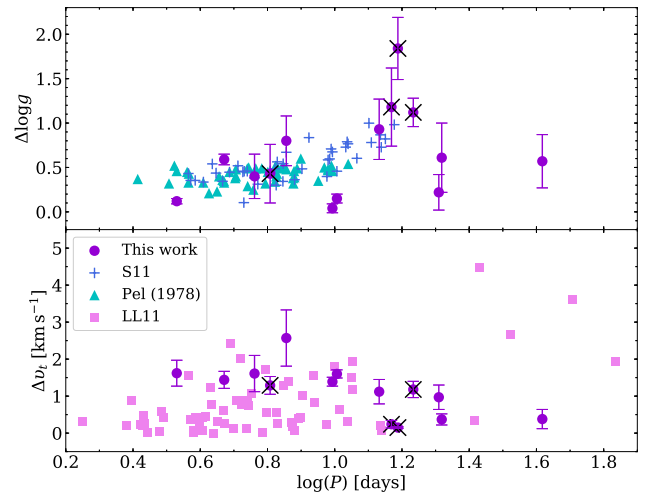


Fig. 4. The same as in Fig. 3, but showing the surface gravity amplitude (top panel) and the microturbulent velocity amplitude (bottom panel).

for which the phase coverage is not optimal. The bottom panel of the same figure shows the comparison between the current microturbulent velocity amplitudes and similar estimates provided by Luck & Lambert (2011, hereinafter LL11) for Cepheids with multiple measurements. The two datasets agree quite well once we take account of the fact that several targets in the LL11 sample only have a few spectra. The same applies for the targets for which we do not have an optimal phase coverage. The surface gravity and microturbulent velocity amplitudes will be discussed in more detail in a forthcoming paper (Urbaneja et al., in prep.) using an independent spectroscopic approach.

4.4. Radial velocity estimates

Radial-velocity measurements were performed for the entire spectroscopic data set, i.e., we also included the spectra for which the S/N was not good enough for the spectroscopic analysis. The radial-velocity curves as a function of the pulsation phase are shown in Fig. 5. Typical radial-velocity errors are around 0.1 km s^{-1} , and normally smaller than 0.5 km s^{-1} , which is often smaller than the symbol size in the figure. The pulsation phase corresponding to each observed spectrum has been computed on the basis of the pulsation period and the photometric data (V-band) available in the literature (Groenewegen 2008; Storm et al. 2011a). However, in most cases the time span between the photometric and the spectroscopic observation is larger than 30 years. On such long time-scales, Cepheids change their period due to evolutionary effects, and by using an outdated period we would introduce a scatter in the folded curves. In order to avoid this effect, we combined the photometric and spectroscopic data to compute a more accurate period, by using a generalized Lomb-Scargle algorithm. The new periods are listed in Table 1, together with the zero-phase reference epoch (T_0) corresponding to maximum light in the V-band.

To validate the radial-velocity amplitudes estimated for the calibrating Cepheids, Fig. 6 shows the comparison between the current values and those provided by S11 for IRSB Galactic Cepheids. Note that only two stars (Y Oph and XX Sgr) are marked with black crosses because the phase coverage is better in the RV plots. The two datasets agree quite well over the entire period range and display the expected V-shape across the Hertzsprung progression ($\log P \sim 1.0$). In this context, we would

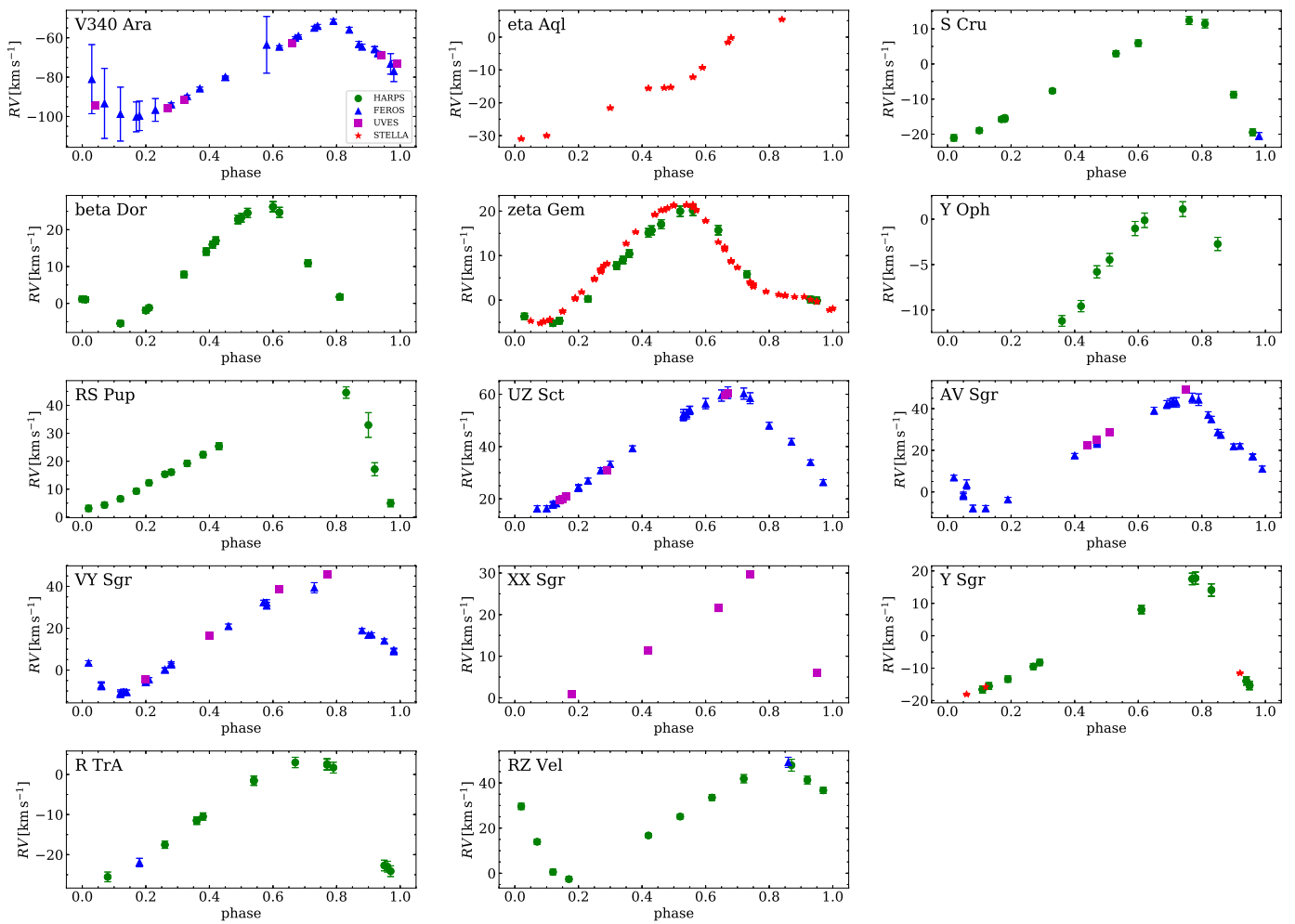


Fig. 5. Radial velocities as a function of the pulsation phase. Measurements based on different spectrographs have been marked with different colors and symbols. The error bars in some cases are smaller than the symbol size.

like to draw the attention to a small sample of Cepheids with periods ranging from $\log P \sim 1.1$ to $\log P \sim 1.6$ that, at fixed period, display radial velocity amplitudes that are on average a factor of two smaller than the bulk of Cepheids. One possible culprit could be the metallicity, since there is preliminary evidence that the amplitudes might decrease when moving into the more metal-poor regime (see Fig. 11 in Genovali et al. 2014). The quality and the homogeneity of the spectra we are collecting will allow us, on a time scale of a few years, to provide more quantitative constraints on this working hypothesis.

5. Iron abundance determinations

The output file of the MOOG code provides the iron abundance for each one of the Fe I and Fe II lines passed as input. The current estimates, when compared with similar estimates available in the literature, present several advantages:

- a) Our sample has between five and more than one hundred spectra per star. This is the reason why the current mean iron abundances have intrinsic errors smaller than 0.1 dex. Before the present work, the number of classical Cepheids for which multiple measurements were available were only a few (see e.g. Luck & Andrievsky 2004; Luck et al. 2008; Romanelli et al. 2008; Genovali et al. 2014).

- b) The current high-resolution spectra cover both the rising and decreasing branch. This means that they cover the pulsation phases during which Cepheids experience the largest variations in effective temperature, surface gravity and microturbulent velocity.
- c) The current calibrating Cepheids roughly cover the period range typical of Galactic classical Cepheids, i.e., from ~ 3 to more than 40 days. This means that the current sample in the Bailey Diagram (luminosity amplitude versus logarithmic period) covers both the low and the large amplitude regime. Moreover, we are also sampling the region of Bump Cepheids. Classical Cepheids with periods ranging from ~ 7 to ~ 10 days display a well defined bump either along the rising (shorter periods) or along the decreasing (longer periods) branch. This is the so-called Hertzsprung progression. The physical mechanisms driving the occurrence of this phenomenon are not fully understood yet, but there is mounting evidence that it is driven by nonlinear phenomena (shocks) across the entire envelope (Bono et al. 2000b).

The individual Fe I and Fe II abundances and their uncertainties, together with the number of lines used are listed in Table 4. Note that the number of lines measured for Fe I lines ranges from a few tens to more than one hundred, while for Fe II it ranges from a few to almost two dozen. These are smaller than the total number of lines available (570 for Fe I and 45 for Fe II) because

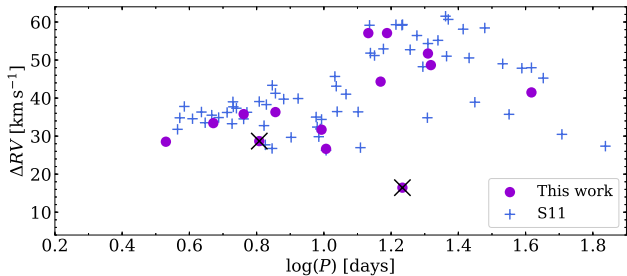


Fig. 6. The same as in Fig. 3, but showing the radial velocity amplitude.

the number of lines measured in each spectrum is limited, e.g., by the wavelength range covered by the instruments, by the intensity of the lines for a given spectral type, by their quality and by the level of blending. Moreover, for each spectrum, we performed a cleaning in order to remove lines that systematically provided too high/low abundances (outside 2σ) when compared with the average abundance.

The mean Fe I and Fe II abundances together with the mean intrinsic parameters are listed in Table 2. A glance at the data given in this table indicates that mean abundances based either on neutral or on ionized iron have similar errors.

The comparison between the current mean iron abundances and similar estimates available in the literature (see Table 1) indicates that they agree quite well within the errors. The iron abundances and their errors listed in Table 1 come from Genovali et al. (2014), in which they derived spectroscopic abundances for the entire sample of CCs based on high-resolution optical spectra. Note that for the measurements for which the original authors did not provide an estimate of the error, they assumed a typical error of 0.1 dex. This means that the difference between the current mean iron abundances and similar estimates available in the literature is, on average, smaller than 1σ . There is only one exception, ζ Gem, for which the difference is of the order of 3σ . The reason for this difference is not clear. ζ Gem is the object with the highest precision, since we analyzed 128 spectra and they cover the entire pulsation cycle. Moreover, the variation of the physical parameters (see Fig. 8) is smooth during both rising and decreasing branch, and both Fe I and Fe II estimates display minimal variations along the entire pulsation cycle of this object (see Fig. 9). Nevertheless, we should notice that ζ Gem is a peculiar Cepheid that has been investigated by Szabados (1983) and classified as a variable star having secular period changes. Indeed, its radial velocity clearly changes with the epoch, as can be seen in Fig. 5, not just due to a velocity offset but real phase shifts seem to be observed, possibly caused by an unseen companion.

To further quantify the difference between the current iron abundances and similar abundances available in the literature, Fig. 7 displays the comparison with the metallicity gradient of Galactic Cepheids provided by Genovali et al. (2014). Data plotted in this figure show some interesting results: *a)* The current sample follows quite well the global metallicity gradient and the new homogeneous mean abundances display a smaller dispersion compared with the literature ones (0.10 vs. 0.12 dex). *b)* The new mean abundances of the four innermost disk objects (V340 Ara, UZ Sct, VY Sgr, AV Sgr) are systematically more metal-poor than literature estimates. This means that the determination of the metallicity gradient in the transition zone between the inner disk and the Bulge (Bono et al. 2013; Genovali et al. 2014) will strongly benefit of more homogeneous and accurate mean iron abundances (Inno et al., in prep.).

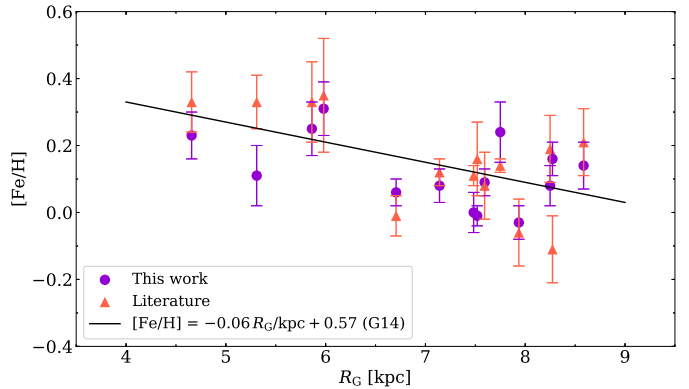


Fig. 7. Iron abundances as a function of Galactocentric distances for the calibrating Cepheids. Values derived in the present work (Table 2) are compared with those from the literature (Table 1). The error bars on our metallicity estimates are the largest value between the uncertainty on the weighted mean and the standard deviation. The metallicity gradient derived by Genovali et al. (2014) is also shown.

5.1. Phase dependence

In the determination of the effective temperature, high standard deviations are not automatically linked to problems in the line-depth measurements. Spectra of stars in the rising phase of their pulsation cycle (i.e., when their effective temperature is increasing) present themselves with intrinsically higher dispersions due to the star's variable nature (they are thus fixed by the physical structure). This could be checked only for the spectra with multiple measurements.

The dependence of the effective temperature on the pulsation phase is shown in Fig. 8. The same figure also shows the variation of the surface gravity and of the microturbulent velocity with the pulsation phase, but the dependence is very weak given the uncertainties. It is worth mentioning that the microturbulent velocity peaks around the pulsation phases in which the Cepheid attains its lowest effective temperatures and soon after, i.e., the phases between ~ 0.5 and $\sim 0.7/0.8$ (see in Fig. 8: S Cru, β Dor, ζ Gem, R TrA). This evidence supports earlier findings by Luck & Andrievsky (2004), Kovtyukh et al. (2005), Andrievsky et al. (2005), and Luck et al. (2008), suggesting that the microturbulent velocity peaks around phases 0.6-0.8. A more quantitative comparison is hampered by the difference in the targets and in the phase coverage. We still lack detailed empirical constraints on the variation of the microturbulent velocity as a function of the pulsation period, and in particular, across the Hertzsprung progression. Homogeneous spectra covering the entire pulsation cycle and a broad period range are highly desired. The same outcome applies to the different approaches suggested to trace the variation of convective motions (Gillet et al. 1999).

Finally, let us note that data plotted in Fig. 9 clearly show that Fe I and Fe II abundances agree quite well within the errors. Moreover and even more importantly, they are independent of the pulsation phase.

6. Summary and final remarks

The quoted results bring forward a few relevant issues worth being discussed in more detail.

- High-resolution, high S/N optical spectra of variable stars allow us to provide precise estimates of both physical parameters and abundances along the pulsation cycle. This means

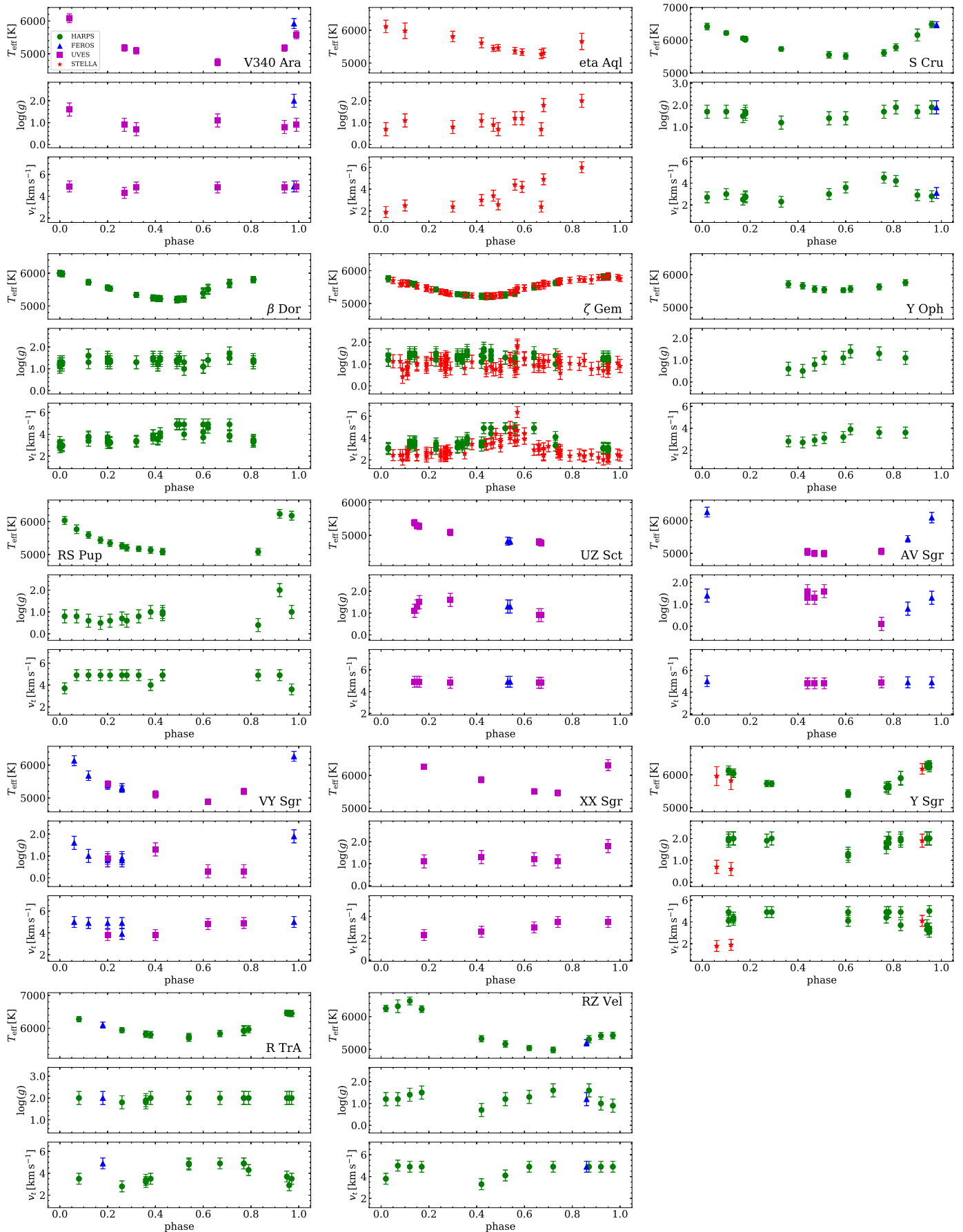


Fig. 8. Atmospheric parameters as a function of the pulsation phase. Measurements from different spectrographs are marked with different colors and symbols. To help with the comparison, the panels are plotted with same y-axis range: 2000 K for T_{eff} , 3 dex for $\log(g)$, and 6 km s^{-1} for v_t .

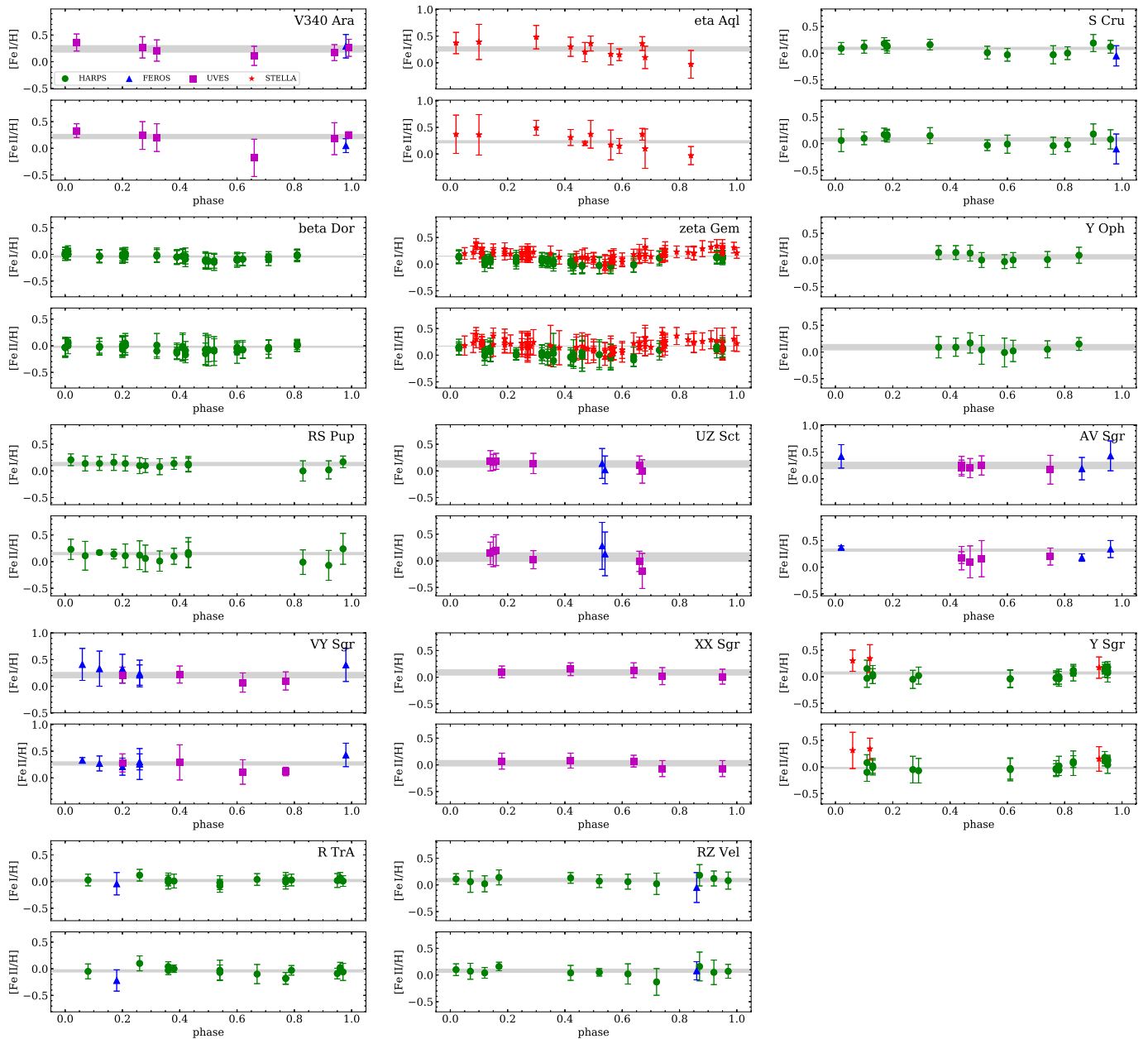


Fig. 9. Abundances from Fe I and Fe II lines as a function of the pulsation phase. The color coding of the different points is the same as in Fig. 8. To help with the comparison, the panels are plotted with same y-axis range: 1.5 dex for both Fe I and Fe II panels. The light grey shaded regions indicate the $\pm 1\sigma$ uncertainty around the weighted mean (from columns 5 and 6 of Table 2).

that spectra collected at random phases can provide solid estimates of Cepheid elemental abundances. This argument applies for relative measurements. Solid constraints on the possible occurrence of systematics in the zero-point of physical parameters and in elemental abundances do require independent spectroscopic approach based either on spectral synthesis and/or on an NLTE analysis.

- b) The observational scenario concerning the LDRs in the NIR regime is lagging compared with the optical one, after the seminal investigation by Sasselov et al. (1989) and Sasselov & Lester (1990a,b) has been hampered by the lack of efficient echelle NIR spectrographs. Fortunately, recent investigations are paving the way for an extension of the LDR into the NIR regime. Fukue et al. (2015) collected H-band spectra with a Subaru high-resolution camera and spectrograph (Kobayashi et al. 2000) for several G- and K-type gi-

ants and supergiants. Interestingly enough, they found that they can provide effective temperatures with an accuracy of the order of 60 K, in spite of the limited range in wavelengths (1.4–1.8 μm) covered by their spectra and the limited number of pairs (nine) they used. Taniguchi et al. (2018), using high-resolution spectra collected with WINERED (Ikeda et al. 2016) in the Y and J bands (0.9–1.35 μm) for ten early G- and M-type giants, found 81 LDR- T_{eff} relations, achieving a precision of 10 K in the best cases. These findings appear as a very promising opportunity for future developments of NIR spectrographs, such as WINERED (see also D’Orazi et al. 2018), CRIRES+ (Follert et al. 2014), and GI-ANO (Origlia et al. 2016).

- c) The new calibrations of the LDRs presented in this paper together with similar calibrations available in the literature span, for the first time, the range in effective temperature cov-

- ered by CCs along their pulsation cycles. However, the range in metallicity covered by the current Cepheids is roughly half a dex around solar metallicity. New extensions into the more metal-poor/metal-rich regime are highly encouraged.
- d) The estimate of the surface gravity using the ionization equilibrium between Fe I and Fe II lines is quite robust, but new approaches are required for metal-poor objects and/or for NIR spectra in which the number of metallic lines is limited. The next Gaia release (DR2), by including accurate estimates of geometrical distances, photometry, and spectroscopy, will constrain the variation of surface gravity for static and variable stars. This is a unique opportunity to constrain possible systematics.
- e) The anti-correlation between microturbulent velocity and effective temperature is quite interesting. Further investigations to derive analytical relations can pave the way to a better understanding of the physical mechanisms (convective transport, non-linear phenomena) driving the efficiency of microturbulent velocity along the pulsation cycle. 1D non-LTE static atmosphere models and 3D dynamical atmosphere models (Chiavassa et al. 2018) would be highly desirable to investigate the physical phenomena affecting line formation and abundances in variable stars.
- f) The current long term variability surveys are discovering hundreds/thousands of classical Cepheids along the obscured regions of the Galactic plane (Udalski et al. 2018, private communication). The new identifications together with fiber multi-object (4MOST, MOONS, APOGEE-South, WEAVE) and slit NIR spectrographs (CRIRES+, WINERED, GI-ANO, CARMENES) will provide a unique opportunity to investigate the chemical enrichment of young stellar populations across the Galactic thin disk.

Acknowledgements. L. Inno acknowledges the Sonderforschungsbereich SFB 881 "The Milky Way System" (subproject A3) of the German Research Foundation (DFG).

References

- Anderson, R. I., Saio, H., Ekström, S., Georgy, C., & Meynet, G. 2016, *A&A*, 591, A8
- Andrievsky, S. M., Bersier, D., Kovtyukh, V. V., et al. 2002a, *A&A*, 384, 140
- Andrievsky, S. M., Kovtyukh, V. V., Luck, R. E., et al. 2002b, *A&A*, 381, 32
- Andrievsky, S. M., Luck, R. E., & Kovtyukh, V. V. 2005, *AJ*, 130, 1880
- Asplund, M., Grevesse, N., Sauval, A. J., & Scott, P. 2009, *ARA&A*, 47, 481
- Baade, W. 1958, *Ricerche Astronomiche*, 5, 165
- Bono, G., Caputo, F., Castellani, V., & Marconi, M. 1999a, *ApJ*, 512, 711
- Bono, G., Caputo, F., Marconi, M., & Musella, I. 2010, *ApJ*, 715, 277
- Bono, G., Castellani, V., & Marconi, M. 2000a, *ApJ*, 529, 293
- Bono, G., Marconi, M., & Stellingwerf, R. F. 1999b, *ApJS*, 122, 167
- Bono, G., Marconi, M., & Stellingwerf, R. F. 2000b, *A&A*, 360, 245
- Bono, G., Matsunaga, N., Inno, L., Lagioia, E. P., & Genovali, K. 2013, in *Astrophysics and Space Science Proceedings*, Vol. 34, *Cosmic Rays in Star-Forming Environments*, ed. D. F. Torres & O. Reimer, 115
- Castelli, F. & Kurucz, R. L. 2004, ArXiv Astrophysics e-prints [[astro-ph/0405087](#)]
- Chiavassa, A., Casagrande, L., Collet, R., et al. 2018, ArXiv e-prints [[arXiv:1801.01895](#)]
- da Silva, R., Lemasle, B., Bono, G., et al. 2016, *A&A*, 586, A125
- Dekker, H., D'Odorico, S., Kaufer, A., Delabre, B., & Kotzlowski, H. 2000, in Proc. SPIE, Vol. 4008, *Optical and IR Telescope Instrumentation and Detectors*, ed. M. Iye & A. F. Moorwood, 534–545
- D'Orazi, V., Magurno, D., Bono, G., et al. 2018, ArXiv e-prints [[arXiv:1802.07314](#)]
- Evans, N. R. 1992, *ApJ*, 384, 220
- Feast, M. W., Laney, C. D., Kinman, T. D., van Leeuwen, F., & Whitelock, P. A. 2008, *MNRAS*, 386, 2115
- Fiorrentino, G., Marconi, M., Musella, I., & Caputo, F. 2007, *A&A*, 476, 863
- Follert, R., Dorn, R. J., Oliva, E., et al. 2014, in Proc. SPIE, Vol. 9147, *Ground-based and Airborne Instrumentation for Astronomy V*, 914719
- François, P., Schuez, O., Conn, B., et al. 2006, *FEROS-II User Manual*, <https://www.eso.org/sci/facilities/lasilla/instruments/feros/doc/manual.pdf>
- Freedman, W. L. & Madore, B. F. 2010, *ARA&A*, 48, 673
- Fukue, K., Matsunaga, N., Yamamoto, R., et al. 2015, *ApJ*, 812, 64
- Gallenle, A., Kervella, P., Mérand, A., et al. 2014, *A&A*, 567, A60
- Genovali, K., Lemasle, B., Bono, G., et al. 2014, *A&A*, 566, A37
- Genovali, K., Lemasle, B., Bono, G., et al. 2013, *A&A*, 554, A132
- Genovali, K., Lemasle, B., da Silva, R., et al. 2015, *A&A*, 580, A17
- Gieren, W., Górska, M., Pietrzynski, G., et al. 2013, *ApJ*, 773, 69
- Gillet, D., Fokin, A. B., Breitfellner, M. G., Mazauric, S., & Nicolas, A. 1999, *A&A*, 344, 935
- Gilmore, G., Randich, S., Asplund, M., et al. 2012, *The Messenger*, 147, 25
- Gray, D. 2005, *The Observation and Analysis of Stellar Photospheres*
- Grevesse, N., Scott, P., Asplund, M., & Sauval, A. J. 2015, *A&A*, 573, A27
- Groenewegen, M. A. T. 2008, *A&A*, 488, 25
- Gustafsson, B., Edvardsson, B., Eriksson, K., et al. 2008, *A&A*, 486, 951
- Heiter, U. & Eriksson, K. 2006, *A&A*, 452, 1039
- Hoffmann, S. L., Macri, L. M., Riess, A. G., et al. 2016, *ApJ*, 830, 10
- Ikeda, Y., Kobayashi, N., Kondo, S., et al. 2016, in Proc. SPIE, Vol. 9908, *Ground-based and Airborne Instrumentation for Astronomy VI*, 99085Z
- Kaufer, A., Stahl, O., Tubbesing, S., et al. 1999, *The Messenger*, 95, 8
- Kervella, P., Bersier, D., Mourard, D., et al. 2004, *A&A*, 428, 587
- Kobayashi, N., Tokunaga, A. T., Terada, H., et al. 2000, in Proc. SPIE, Vol. 4008, *Optical and IR Telescope Instrumentation and Detectors*, ed. M. Iye & A. F. Moorwood, 1056–1066
- Kovtyukh, V., Lemasle, B., Chekhonadskikh, F., et al. 2016, *MNRAS*, 460, 2077
- Kovtyukh, V. V. 2007, *MNRAS*, 378, 617
- Kovtyukh, V. V. & Andrievsky, S. M. 1999, *A&A*, 350, L55
- Kovtyukh, V. V., Andrievsky, S. M., Belik, S. I., & Luck, R. E. 2005, *AJ*, 129, 433
- Kovtyukh, V. V., Andrievsky, S. M., Luck, R. E., & Gorlova, N. I. 2003a, *A&A*, 401, 661
- Kovtyukh, V. V. & Gorlova, N. I. 2000, *A&A*, 358, 587
- Kovtyukh, V. V., Soubiran, C., Belik, S. I., & Gorlova, N. I. 2003b, *A&A*, 411, 559
- Kraft, R. P. 1956, *PASP*, 68, 137
- Kraft, R. P. 1957, *ApJ*, 125, 336
- Krockenberger, M., Sasselov, D., Noyes, R., et al. 1998, in *Astronomical Society of the Pacific Conference Series*, Vol. 154, *Cool Stars, Stellar Systems, and the Sun*, ed. R. A. Donahue & J. A. Bookbinder, 791
- Kurucz, R. L., Furenlid, I., Brault, J., & Testerman, L. 1984, *Solar flux atlas from 296 to 1300 nm*
- Lemasle, B., François, P., Bono, G., et al. 2007, *A&A*, 467, 283
- Lemasle, B., François, P., Genovali, K., et al. 2013, *A&A*, 558, A31
- Lemasle, B., François, P., Piersimoni, A., et al. 2008, *A&A*, 490, 613
- Lemasle, B., Groenewegen, M., Grebel, E., et al. 2017, *A&A*, submitted
- Li Causi, G., Antonucci, S., Bono, G., et al. 2013, *A&A*, 549, A64
- Luck, R. E. & Andrievsky, S. M. 2004, *AJ*, 128, 343
- Luck, R. E., Andrievsky, S. M., Fokin, A., & Kovtyukh, V. V. 2008, *AJ*, 136, 98
- Luck, R. E., Andrievsky, S. M., Kovtyukh, V. V., Gieren, W., & Graczyk, D. 2011, *AJ*, 142, 51
- Luck, R. E. & Lambert, D. L. 2011, *AJ*, 142, 136
- Luck, R. E., Moffett, T. J., Barnes, III, T. G., & Gieren, W. P. 1998, *AJ*, 115, 605
- Macri, L. M., Ngeow, C.-C., Kanbur, S. M., Mahzooni, S., & Smitka, M. T. 2015, *AJ*, 149, 117
- Marconi, M., Musella, I., & Fiorentino, G. 2005, *ApJ*, 632, 590
- Mathias, P., Gillet, D., Fokin, A. B., et al. 2006, *A&A*, 457, 575
- Mayor, M., Pepe, F., Queloz, D., et al. 2003, *The Messenger*, 114, 20
- Mérand, A., Kervella, P., Breitfelder, J., et al. 2015, *A&A*, 584, A80
- Nardetto, N., Gieren, W., Kervella, P., et al. 2009, *A&A*, 502, 951
- Orlighia, L., Oliva, E., Sanna, N., et al. 2016, *A&A*, 585, A14
- Pel, J. W. 1978, *A&A*, 62, 75
- Pietrzynski, G., Graczyk, D., Gieren, W., et al. 2013, *Nature*, 495, 76
- Preston, G. W. 1964, *ARA&A*, 2, 23
- Preston, G. W., Smak, J., & Paczynski, B. 1965, *ApJS*, 12, 99
- Randich, S., Gilmore, G., & Gaia-ESO Consortium. 2013, *The Messenger*, 154, 47
- Riess, A. G., Macri, L. M., Hoffmann, S. L., et al. 2016, *ApJ*, 826, 56
- Romanillo, M., Primas, F., Mottini, M., et al. 2008, *A&A*, 488, 731
- Rybchikova, T., Piskunov, N., Kurucz, R. L., et al. 2015, *Phys. Scr.*, 90, 054005
- Sasselov, D. D., Fieldus, M. S., & Lester, J. B. 1989, *ApJ*, 337, L29
- Sasselov, D. D. & Lester, J. B. 1990a, *ApJ*, 360, 227
- Sasselov, D. D. & Lester, J. B. 1990b, *ApJ*, 362, 333
- Scott, P., Asplund, M., Grevesse, N., Bergemann, M., & Sauval, A. J. 2015a, *A&A*, 573, A26
- Scott, P., Grevesse, N., Asplund, M., et al. 2015b, *A&A*, 573, A25
- Sneden, C. 2002, *The MOOG code*, <http://www.as.utexas.edu/~chris/moog.html>
- Soszyński, I., Udalski, A., Szymański, M. K., et al. 2017, *Acta Astron.*, 67, 103
- Sousa, S. G., Santos, N. C., Adibekyan, V., Delgado-Mena, E., & Israelián, G. 2015, *A&A*, 577, A67

- Sousa, S. G., Santos, N. C., Israelian, G., Mayor, M., & Monteiro, M. J. P. F. G. 2007, A&A, 469, 783
- Storm, J., Gieren, W., Fouqué, P., et al. 2011a, A&A, 534, A94
- Storm, J., Gieren, W., Fouqué, P., et al. 2011b, A&A, 534, A95
- Strassmeier, K. G., Granzer, T., Weber, M., et al. 2004, Astronomische Nachrichten, 325, 527
- Strassmeier, K. G., Granzer, T., Weber, M., et al. 2010, Advances in Astronomy, 2010, 970306
- Struve, O. 1944, The Observatory, 65, 257
- Szabados, L. 1983, Ap&SS, 96, 185
- Szabados, L. 1990, MNRAS, 242, 285
- Szabados, L. 2003, Information Bulletin on Variable Stars, 5394
- Taniguchi, D., Matsunaga, N., Kobayashi, N., et al. 2018, MNRAS, 473, 4993
- Vasilyev, V., Ludwig, H.-G., Freytag, B., Lemasle, B., & Marconi, M. 2017a, A&A, 606, A140
- Vasilyev, V., Ludwig, H.-G., Freytag, B., Lemasle, B., & Marconi, M. 2017b, ArXiv e-prints [[arXiv:1711.00236](https://arxiv.org/abs/1711.00236)]
- Wallerstein, G. 1972, PASP, 84, 656
- Wallerstein, G. 1979, PASP, 91, 772
- Wallerstein, G., Albright, M. B., & Ritchey, A. M. 2015, PASP, 127, 503
- Weber, M., Granzer, T., & Strassmeier, K. G. 2012, in Proc. SPIE, Vol. 8451, Software and Cyberinfrastructure for Astronomy II, 84510K

Table 3. New and old Line Depth Ratios (LDRs) adopted for effective temperature estimates.

λ_1 [Å]	Ion	λ_2 [Å]	Ion	ΔT_{eff} [K]	a	b	c	d	e	f	Function	Ref.
5348.30	Cr I	5554.89	Fe I	7200-7700	8120	-919.996	$a + br$	2
5348.30	Cr I	5565.71	Fe I	7200-7700	7940	-646.94	$a + br$	2
5373.71	Fe I	5501.46	Fe I	7200-7700	6757	1603.21	$a + br$	2
5410.91	Fe I	5501.46	Fe I	7200-7700	6748	463.441	$a + br$	2
5497.52	Fe I	5554.89	Fe I	7200-7700	8065	-295.956	$a + br$	2
5501.46	Fe I	5554.89	Fe I	7200-7700	8490	-809.128	$a + br$	2
5501.46	Fe I	5565.71	Fe I	7200-7700	8487	-805.207	$a + br$	2
5501.46	Fe I	5633.97	Fe I	7200-7700	8473	-557.534	$a + br$	2
5506.78	Fe I	5554.89	Fe I	7200-7700	8673	-767.096	$a + br$	2
5506.78	Fe I	5565.71	Fe I	7200-7700	8986	-968.498	$a + br$	2
5506.78	Fe I	5633.97	Fe I	7200-7700	8639	-521.982	$a + br$	2
5578.72	Ni I	5645.62	Si I	5400-6300	9486.76	0.653644	0.283943	$ab^{1/r}r^c$	2
5578.72	Ni I	5805.23	Ni I	5600-6750	7343	-975.039	-74.7727	$a + br + cr^2$	2
5670.86	V I	5690.43	Si I	3700-6400	7113	-7600.38	11646.9	-9095.52	3251.54	-433.007	$a + br + cr^2 + dr^3 + er^4 + fr^5$	2
5754.68	Ni I	5772.15	Si I	7200-7700	8101	-941.716	$a + br$	2
5754.68	Ni I	5772.15	Si I	5400-7000	7553	-906.095	-319.209	$a + br + cr^2$	2
5772.15	Si I	5778.47	Fe I	5000-6500	4870.26	0.991324	0.177759	$ab^{1/r}r^c$	2
5772.15	Si I	5778.47	Fe I	3600-5000	2733	1889.61	$a + br$	2
5772.15	Si I	5847.00	Ni I	3750-6400	5600.3858	0.859917	7.6436205	$ab^{1/r}r^c$	3
5772.15	Si I	5866.45	Ti I	3750-6400	5844.6836	0.89753238	0.36660117	$ab^{1/r}r^c$	3
5778.47	Fe I	5793.08	Si I	4700-6550	5150.2198	-0.19395103	-0.20263094	$a(r - b)^c$	3
5793.08	Si I	5793.92	Fe I	4600-6900	1828	4179.03	-1318.34	150.31	$a + br + cr^2 + dr^3$	2
5793.08	Si I	5847.00	Ni I	3750-6400	5292.4677	188.04705	-431.74828	$a + br + c/r^2$	3
5793.08	Si I	5866.45	Ti I	3750-6900	6385.3741	0.85596741	0.047715024	$ab^{1/r}r^c$	3
5809.25	Fe I	6046.00	S I	5300-6900	7849	-2708.78	1124.64	-187.28	$a + br + cr^2 + dr^3$	2
5809.25	Fe I	6052.67	S I	5450-6900	7543	-2173.24	763.632	-96.4729	$a + br + cr^2 + dr^3$	2
5847.00	Ni I	5862.36	Fe I	4800-6400	4732.753	0.9950455	-0.14769983	$ab^{1/r}r^c$	3
5847.00	Ni I	5905.67	Fe I	4800-6350	6972.3012	-4507.1987	3736.2682	-1279.5186	$a + br + cr^2 + dr^3$	3
5847.00	Ni I	5987.05	Fe I	4800-6350	6952.0126	-5341.52	5624.8112	-2521.265	$a + br + cr^2 + dr^3$	3
5847.00	Ni I	6003.03	Fe I	4800-6350	6988.9083	-6964.1741	9499.6138	-5413.4344	$a + br + cr^2 + dr^3$	3
5847.00	Ni I	6046.00	S I	4800-6900	5548.4816	0.9885989	-0.081945655	$ab^{1/r}r^c$	3
5862.36	Fe I	5866.45	Ti I	3750-6400	6394.1552	0.7536621	0.033678894	$ab^{1/r}r^c$	3
5866.45	Ti I	5905.67	Fe I	4800-6350	6727.9816	-597.326	-1541.8658	727.53509	$a + br + cr^2 + dr^3$	3
5866.45	Ti I	5983.69	Fe I	4800-6900	0.0001341342	7.89E-05	-1.43E-05	$1/(a + br + cr^2)$	3
5866.45	Ti I	5984.79	Fe I	4800-6900	6164.4205	0.79631902	-0.062253009	$ab^{1/r}r^c$	3
5866.45	Ti I	6003.03	Fe I	4800-6900	7219.8944	-3585.8283	1210.6378	$a + br + cr^2$	3
5866.45	Ti I	6021.79	Mn I	4800-6700	7201.1881	-3234.7364	754.27062	$a + br + cr^2$	3
5866.45	Ti I	6046.00	S I	4700-6900	6034.8217	-0.27055898	-0.14115708	$ar(r - b)^c$	3
5866.45	Ti I	6055.99	Fe I	4800-6900	7099.5674	-2781.3457	770.38101	$a + br + cr^2$	3
5934.66	Fe I	6046.00	S I	7200-7700	8390	-978.164	$a + br$	2
5934.66	Fe I	6052.67	S I	7200-7700	8221	-918.937	$a + br$	2
5956.70	Fe I	5983.69	Fe I	3700-6900	7286	-2865.02	1353.68	-396.557	$a + br + cr^2 + dr^3$	2
5956.70	Fe I	6142.49	Si I	3750-6450	7052.7128	-1014.7929	97.242351	-3.3812526	$a + br + cr^2 + dr^3$	3
5987.05	Fe I	6216.37	V I	3600-5700	1179	6441.65	-3564.96	709.834	$a + br + cr^2 + dr^3$	2
6003.03	Fe I	6052.67	S I	5550-7000	6283.25	1.083756	-0.1341008	$ab^{1/r}r^c$	2
6003.03	Fe I	6052.67	S I	7200-7700	8037	-551.182	$a + br$	2
6007.96	Fe I	6082.72	Fe I	3750-6350	5459.2622	305.72716	-787.01683	$a + br + c/r^2$	3
6008.56	Fe I	6046.00	S I	5600-7000	7155.97	-0.241376	ar^b	2
6021.79	Mn I	6046.00	S I	5700-7000	7944	-1437.72	260.697	-19.1727	$a + br + cr^2 + dr^3$	2
6021.79	Mn I	6052.67	S I	5700-7000	7749	-1312.04	221.004	-13.474	$a + br + cr^2 + dr^3$	2
6024.07	Fe I	6082.72	Fe I	3750-6550	5388.3579	150.09207	-1263.9396	$a + br + c/r^2$	3
6039.73	V I	6046.00	S I	3700-5400	5569	-345.093	5.36966	$a + br + cr^2$	2
6039.73	V I	6078.50	Fe I	3750-5400	5590.5654	-1140.171	-197.64575	139.85301	$a + br + cr^2 + dr^3$	3
6039.73	V I	6079.02	Fe I	3750-5750	5349.3333	0.87139818	-0.06060133	$ab^{1/r}r^c$	3
6039.73	V I	6091.92	Si I	3800-6050	5060.286	0.97817533	-0.11128624	$ab^{1/r}r^c$	3
6039.73	V I	6145.02	Si I	3750-5650	5144.3594	0.95420384	-0.073702513	$ab^{1/r}r^c$	3
6039.73	V I	6155.14	Si I	3750-5450	-555860.5	-92075392	-16835.861	-3465.0764	$(a + br)/(1 + cr + dr^2)$	3

continued on next page

Table 3. continued.
Article number, page 16 of 25

λ_1 [Å]	Ion	λ_2 [Å]	Ion	ΔT_{eff} [K]	a	b	c	d	e	f	Function	Ref.
6039.73	V I	6237.33	Si I	3750-5500	5188.6032	0.89874901	-0.055517417	$ab^r r^c$	3
6046.00	S I	6062.89	Fe I	4600-6400	5470.5386	0.99518466	0.10524197	$ab^r r^c$	3
6046.00	S I	6081.44	V I	4450-6400	5166.8456	-0.15189352	0.10673444	$a(r - b)^c$	3
6046.00	S I	6082.72	Fe I	4450-6550	5786.2114	0.98639057	0.1266466	$ab^r r^c$	3
6046.00	S I	6085.27	Fe I	4450-6900	5846.0931	0.98556293	0.13541182	$ab^r r^c$	3
6046.00	S I	6086.29	Ni I	4800-6800	6156.77	0.954343	0.218591	$ab^r r^c$	2
6046.00	S I	6091.18	Ti I	4450-6350	4581.1358	619.83166	-82.470124	3.8980452	$a + br + cr^2 + dr^3$	3
6046.00	S I	6108.12	Ni I	4800-6700	6384.08	0.97804	0.0987979	$ab^{1/r} r^c$	2
6046.00	S I	6126.22	Ti I	4450-6650	4243.1981	6981.8997	1.0296664	-0.0051885512	$(a + br)/(1 + cr + dr^2)$	3
6046.00	S I	6130.17	Ni I	4600-6350	4305.295	976.14392	-64.570196	-18.376814	$a + br + cr^2 + dr^3$	3
6046.00	S I	6151.62	Fe I	4450-6900	3802.3885	16046.227	2.3423486	-0.030215793	$(a + br)/(1 + cr + dr^2)$	3
6046.00	S I	6165.37	Fe I	4950-6500	5953.195	0.9938577	0.153777	$ab^{1/r} r^c$	2
6046.00	S I	6176.81	Ni I	7200-7700	6075	877.871	$a + br$	2
6046.00	S I	6180.22	Fe I	4950-6700	6383.75	0.96151	0.170212	$ab^r r^c$	2
6046.00	S I	6215.15	Fe I	7200-7700	6896	358.445	$a + br$	2
6046.00	S I	6240.66	Fe I	4450-6900	4016.0153	12659.012	1.8004153	-0.011523382	$(a + br)/(1 + cr + dr^2)$	3
6046.00	S I	6243.11	V I	4450-6350	5536.7477	0.99676933	0.089085045	$ab^r r^c$	3
6046.00	S I	6258.10	Ti I	4750-6700	6037.88	0.98653	0.110763	$ab^{1/r} r^c$	2
6052.67	S I	6082.72	Fe I	4600-6550	5731.2095	0.99327876	0.096572399	$ab^{1/r} r^c$	3
6052.67	S I	6108.12	Ni I	5250-6800	6293.6	0.984529	0.129272	$ab^r r^c$	2
6052.67	S I	6108.12	Ni I	7200-7700	6558	246.382	$a + br$	2
6052.67	S I	6122.23	Cai	7200-7700	6905	1649.06	$a + br$	2
6052.67	S I	6136.61	Fe I	7200-7700	6866	1219.4	$a + br$	2
6052.67	S I	6151.62	Fe I	5000-6800	6074.89	0.984276	0.127801	$ab^r r^c$	2
6052.67	S I	6162.18	Cai	7200-7700	6821	2178.43	$a + br$	2
6052.67	S I	6176.81	Ni I	7200-7700	7016	265.574	$a + br$	2
6052.67	S I	6180.22	Fe I	5000-6700	6224.77	0.979038	0.142497	$ab^r r^c$	2
6052.67	S I	6215.15	Fe I	7200-7700	7025	239.858	$a + br$	2
6052.67	S I	6219.28	Fe I	7200-7700	7140	302.498	$a + br$	2
6052.67	S I	6240.66	Fe I	5050-6750	6057.77	0.986549	0.126622	$ab^r r^c$	2
6052.67	S I	6258.10	Ti I	5000-6750	5924	688.557	$a + b \log r$	2
6055.99	Fe I	6062.89	Fe I	3700-4850	9851.19	0.473424	-0.446733	$ab^{1/r} r^c$	2
6055.99	Fe I	6062.89	Fe I	5000-6000	-21.6837	418.865	4532	$a + br + cr^2$	2
6055.99	Fe I	6082.72	Fe I	3750-3550	5357.431	264.82251	-770.39303	$a + br + c/r^2$	3
6055.99	Fe I	6085.27	Fe I	4900-6750	5140.04	0.96892	0.257266	$ab^r r^c$	2
6055.99	Fe I	6085.27	Fe I	3600-4900	2405	2480.21	$a + br$	2
6055.99	Fe I	6151.62	Fe I	3750-6700	5765.9039	289.50467	-885.53492	$a + br + c/r^2$	3
6055.99	Fe I	6180.22	Fe I	3750-6550	6311.9278	167.30491	-1248.4987	$a + br + c/r^2$	3
6055.99	Fe I	6243.11	V I	3750-6350	5143.6204	180.91218	-340.54146	$a + br + c/r^2$	3
6062.89	Fe I	6078.50	Fe I	4800-6400	7023.5296	-6273.8558	6896.536	-2897.7313	$a + br + cr^2 + dr^3$	3
6062.89	Fe I	6091.92	Si I	3800-6500	5594.0551	0.95024411	-0.11399896	$ab^r r^c$	3
6062.89	Fe I	6145.02	Si I	4750-6500	7037.1654	-3469.1523	2026.3339	-438.42083	$a + br + cr^2 + dr^3$	3
6062.89	Fe I	6237.33	Si I	4750-6350	6986.3819	-4788.9303	4169.7261	-1434.1114	$a + br + cr^2 + dr^3$	3
6078.50	Fe I	6082.72	Fe I	3750-6400	5293.1184	268.82143	-733.04741	$a + br + c/r^2$	3
6078.50	Fe I	6085.27	Fe I	4900-6800	5935.8	0.824949	0.0896904	$ab^{1/r} r^c$	2
6078.50	Fe I	6085.27	Fe I	3600-4950	2484	2374.49	$a + br$	2
6078.50	Fe I	6243.11	V I	3750-6350	5152.999	173.02512	-349.42793	$a + br + c/r^2$	3
6078.50	Fe I	6258.10	Ti I	3750-6400	6707.9691	0.74607455	0.057018238	$ab^{1/r} r^c$	3
6078.50	Fe I	6258.71	Ti I	3900-6900	8385.9963	0.57382889	$ar/(b + r)$	3
6081.44	V I	6145.02	Si I	3750-5700	547550.54	13399692	2584.0445	211.68131	$(a + br)/(1 + cr + dr^2)$	3
6081.44	V I	6155.14	Si I	3750-5500	5751.571	-1528.4472	503.44595	-90.6585	$a + br + cr^2 + dr^3$	3
6081.44	V I	6176.81	Ni I	3800-5500	5537.8688	-984.85259	11.202499	$a + br + c/r^2$	3
6081.44	V I	6237.33	Si I	3750-5900	1264810.5	55029420	10277.115	1582.781	$(a + br)/(1 + cr + dr^2)$	3
6081.44	V I	6243.81	Si I	3750-5900	1276671.6	41437376	7844.3312	1018.2459	$(a + br)/(1 + cr + dr^2)$	3
6082.72	Fe I	6091.92	Si I	3800-6550	6255.7979	0.91578628	-0.089526206	$ab^r r^c$	3
6082.72	Fe I	6125.03	Si I	4800-6550	7189.7511	-1996.0635	425.19285	$a + br + cr^2$	3
6082.72	Fe I	6142.49	Si I	3750-6550	8026.8322	-1.2495207	-0.4271677	$a(r - b)^c$	3

continued on next page

Table 3. continued.

λ_1 [Å]	Ion	λ_2 [Å]	Ion	ΔT_{eff} [K]	a	b	c	d	e	f	Function	Ref.
6082.72	Fe I	6145.02	Si I	3750-6550	6039.2179	0.9182164	-0.098249267	$ab^r r^c$	3
6082.72	Fe I	6155.14	Si I	4800-6550	5145.1625	-0.14258724	-0.20952186	$a(r - b)^c$	3
6082.72	Fe I	6170.49	Fe I	4800-6600	5771.2091	-0.55350322	-0.42594585	$a(r - b)^c$	3
6082.72	Fe I	6237.33	Si I	3750-6550	7072.4147	-3032.6104	1513.9486	-371.04912	$a + br + cr^2 + dr^3$	3
6082.72	Fe I	6243.81	Si I	3750-6550	7196.6943	-2751.3448	1087.5405	-213.44259	$a + br + cr^2 + dr^3$	3
6085.27	Fe I	6086.29	Ni I	4200-6700	7683	-2129.69	114.528	$a + br + cr^2$	2
6085.27	Fe I	6091.92	Si I	3800-6650	7252.8278	-1703.6908	311.72639	-21.895353	$a + br + cr^2 + dr^3$	3
6085.27	Fe I	6142.49	Si I	3750-6650	7634.692	630.77421	0.44872922	-0.018371584	$(a + br)/(1 + cr + dr^2)$	3
6085.27	Fe I	6155.14	Si I	3750-6900	5708.4483	0.8720183	-0.10554208	$ab^r r^c$	3
6085.27	Fe I	6237.33	Si I	3750-6900	8222.8194	-1.2533326	-0.56289765	$a(r - b)^c$	3
6090.21	V I	6091.92	Si I	3700-5800	6585	-1215.97	185.711	-11.2669	$a + br + cr^2 + dr^3$	2
6090.21	V I	6155.14	Si I	3700-5750	5638.22	0.866727	-0.0731712	$ab^r r^c$	2
6090.21	V I	6330.86	Fe I	3700-5550	7359	-1844.03	213.264	$a + br + cr^2$	2
6091.18	Ti I	6125.03	Si I	4800-6350	4277.4717	1.139652	-0.22374728	$ab^r r^c$	3
6091.18	Ti I	6145.02	Si I	3750-5750	4980.2378	0.96649545	-0.11349399	$ab^r r^c$	3
6091.18	Ti I	6155.14	Si I	3750-5450	5153.6733	0.8565174	-0.054459935	$ab^r r^c$	3
6091.18	Ti I	6237.33	Si I	3750-5750	4928.1186	0.91700085	-0.1017638	$ab^r r^c$	3
6091.92	Si I	6219.28	Fe I	7200-7700	6935	1346.25	$a + br$	2
6091.92	Si I	6243.11	V I	3800-6350	5625.0556	0.96931038	0.092095843	$ab^{1/r} r^c$	3
6093.14	Co I	6093.66	Fe I	3700-6200	6679	-3868.72	3130.89	-1022.74	$a + br + cr^2 + dr^3$	2
6108.12	Ni I	6125.03	Si I	5600-7000	7910.42	0.821822	0.0421413	$ab^r r^c$	2
6108.12	Ni I	6145.02	Si I	4000-7000	7598	-1309.78	90.231	$a + br + cr^2$	2
6108.12	Ni I	6155.14	Si I	4600-6900	7023.0844	-614.59734	-1541.5092	661.13611	$a + br + cr^2 + dr^3$	3
6108.12	Ni I	6237.33	Si I	5400-7000	7549	-1908.86	283.413	$a + br + cr^2$	2
6125.03	Si I	6126.22	Ti I	4400-6650	5571.4418	0.95872488	0.2433342	$ab^r r^c$	3
6125.03	Si I	6151.62	Fe I	5600-6600	6834.79	0.892416	0.0563776	$ab^{1/r} r^c$	2
6125.03	Si I	6243.11	V I	4800-6350	4414.6542	1216.2187	-311.79239	31.88682	$a + br + cr^2 + dr^3$	3
6125.03	Si I	6358.69	Fe I	7200-7700	8295	-505.937	$a + br$	2
6126.22	Ti I	6145.02	Si I	3750-6900	5541.4767	-0.22966992	-0.23199881	$a(r - b)^c$	3
6126.22	Ti I	6155.14	Si I	3750-6550	5192.2074	0.91920445	-0.12146185	$ab^r r^c$	3
6126.22	Ti I	6237.33	Si I	3750-6550	5343.9359	0.92516671	-0.12840343	$ab^r r^c$	3
6128.99	Ni I	6237.33	Si I	3750-6550	6934.9822	-3307.7598	2018.2402	-577.34869	$a + br + cr^2 + dr^3$	3
6135.36	V I	6142.49	Si I	3700-5300	5575	-656.539	35.5005	$a + br + cr^2$	2
6135.36	V I	6237.33	Si I	3750-5650	5193.125	0.8986041	-0.044948334	$ab^r r^c$	3
6136.61	Fe I	6243.11	V I	3750-6350	5226.9903	78.711256	-1353.7489	$a + br + c/r^2$	3
6142.49	Si I	6243.11	V I	3750-6350	5575.6374	0.97029759	0.097815165	$ab^{1/r} r^c$	3
6145.02	Si I	6151.62	Fe I	3750-6700	7414.7921	0.24285202	$ar/(b + r)$	3
6145.02	Si I	6180.22	Fe I	3700-5000	2382	5416.72	$a + br$	2
6145.02	Si I	6243.11	V I	3750-6350	5515.3062	0.96712503	0.09179199	$ab^{1/r} r^c$	3
6145.02	Si I	6258.10	Ti I	3700-6700	2870	5476.94	-3256.51	800.595	$a + br + cr^2 + dr^3$	2
6150.16	V I	6237.33	Si I	3700-4900	5505	-770.29	$a + br$	2
6150.16	V I	6380.75	Fe I	3700-4800	6126	-1611.92	$a + br$	2
6151.62	Fe I	6155.14	Si I	3750-6900	6727.799	0.7737723	-0.036684239	$ab^r r^c$	3
6151.62	Fe I	6237.33	Si I	3750-6900	7156.5565	-1767.765	146.61902	$a + br + cr^2$	3
6155.14	Si I	6180.22	Fe I	3750-6900	-14407.078	75426.24	10.641479	-0.09935597	$(a + br)/(1 + cr + dr^2)$	3
6155.14	Si I	6240.66	Fe I	3750-6900	6784.9875	0.76711376	0.026378813	$ab^{1/r} r^c$	3
6155.14	Si I	6243.11	V I	3750-6350	5393.2959	0.92019335	0.073807492	$ab^{1/r} r^c$	3
6155.14	Si I	6358.69	Fe I	3700-6700	6642.5	0.85674	0.086193	$ab^{1/r} r^c$	2
6170.49	Fe I	6180.22	Fe I	5150-6850	380	7413.41	-3207.31	501.652	$a + br + cr^2 + dr^3$	2
6176.81	Ni I	6243.11	V I	3800-6350	5094.4861	234.05509	-315.52803	$a + br + c/r^2$	3
6176.81	Ni I	6258.10	Ti I	3700-6200	6317.32	0.812411	0.611525	$ab^r r^c$	2
6176.81	Ni I	6261.10	Ti I	4700-6700	2011	3758	-753.8	$a + br + cr^2$	1
6180.22	Fe I	6237.33	Si I	3750-6900	7361.1377	-1749.5269	52.616694	$a + br + cr^2$	3
6189.01	Co I	6237.33	Si I	3750-5400	5602.0793	-1172.9134	370.85881	-109.56462	$a + br + cr^2 + dr^3$	3
6189.01	Co I	6244.48	Si I	3750-5500	5421.6284	-616.52128	9.4613246	$a + br + c/r^2$	3
6200.32	Fe I	6237.33	Si I	5300-6900	7936	-1668.99	$a + br$	2
6219.28	Fe I	6414.99	Si I	7200-7700	8068	-364.285	$a + br$	2

continued on next page

λ_1 [Å]	Ion	λ_2 [Å]	Ion	ΔT_{eff} [K]	a	b	c	d	e	f	Function	Ref.
6232.65	Fe I	6243.11	V I	3750-6350	5105.7991	177.4715	-513.57204	$a + br + c/r^2$	3
6237.33	Si I	6240.66	Fe I	3750-6900	32620441	-168828320	-25019.24	389.82997	$(a + br)/(1 + cr + dr^2)$	3
6237.33	Si I	6243.11	V I	3750-6350	5509.5994	0.92783258	0.074721402	$ab^{1/r}r^c$	3
6237.33	Si I	6258.10	Ti I	4700-6700	6691.94	0.808588	0.0677634	$ab^{1/r}r^c$	2
6237.33	Si I	6258.71	Ti I	4800-6700	2379	5481.69	-2484.04	406.352	$a + br + cr^2 + dr^3$	2
6237.33	Si I	6358.69	Fe I	3750-6900	7336.2706	0.82039503	0.021229756	$ab^{1/r}r^c$	3
6240.66	Fe I	6243.81	Si I	3750-6900	7448.8726	0.77089127	ab^r	3
6240.66	Fe I	6244.48	Si I	4500-6900	7340.2	0.793709	-0.0153904	$ab^r r^c$	2
6240.66	Fe I	6414.99	Si I	4000-6900	6892.895	0.84853114	-0.039046311	$ab^r r^c$	3
6243.11	V I	6243.81	Si I	4800-5900	6561.787	-2261.2405	1032.1541	-171.36594	$a + br + cr^2 + dr^3$	3
6243.11	V I	6244.48	Si I	4800-5900	6564.3353	-2186.4868	956.13517	-145.40885	$a + br + cr^2 + dr^3$	3
6243.11	V I	6414.99	Si I	4800-5900	6478.4211	-1881.5917	820.5678	-141.74283	$a + br + cr^2 + dr^3$	3
6243.11	V I	6439.08	Ca I	4000-5500	6265.953	-4949.8037	7534.6692	-4708.8282	$a + br + cr^2 + dr^3$	3
6243.81	Si I	6261.10	Ti I	3700-5600	2952	3689.04	-1068.2	$a + br + cr^2$	2
6243.81	Si I	6358.69	Fe I	3700-7000	7757.8	0.81203	0.00385864	$ab^{1/r}r^c$	2
6244.48	Si I	6258.10	Ti I	4700-6600	2199	6096	3216	634.3	$a + br + cr^2 + dr^3$	1
6327.60	Ni I	6414.99	Si I	3700-6900	6080.41	0.906332	-0.0951967	$ab^r r^c$	2
6330.13	Cr I	6330.86	Fe I	4700-6700	7190	-2042	307.6	$a + br + cr^2$	1
6330.13	Cr I	6414.99	Si I	3700-6000	5526.66	0.937233	-0.111614	$ab^r r^c$	2
6355.04	Fe I	6414.99	Si I	3700-7000	7780	-1298.65	$a + br$	2
6355.04	Fe I	6419.98	Fe I	3700-7000	7433	-1541.58	7.58844	-464.06	$a + br + cr^2 + dr^3$	2
6358.69	Fe I	6414.99	Si I	4400-7000	7527	-1283.15	99.1835	$a + br + cr^2$	2
6358.69	Fe I	6419.98	Fe I	3700-7000	7482	-2075.08	143.949	$a + br + cr^2$	2
6392.55	Fe I	6414.99	Si I	3700-6200	6889	-4485.89	4193.86	-1917.35	294.546	...	$a + br + cr^2 + dr^3 + er^4$	2
6414.99	Si I	6498.95	Fe I	4200-6550	6204.5377	0.91929415	0.066862673	$ab^{1/r}r^c$	3
6498.95	Fe I	6597.61	Fe I	4850-6600	8132	-4988.98	4606.31	-2274.22	408.814	...	$a + br + cr^2 + dr^3 + er^4$	2
6538.60	S I	6609.12	Fe I	5600-7000	4943	4959.69	-4809.9	1698.54	$a + br + cr^2 + dr^3$	2
6597.61	Fe I	6608.03	Fe I	4700-6500	3853	1195	-225	15.9	$a + br + cr^2 + dr^3$	1
6608.03	Fe I	6721.85	Si I	4700-6550	0.0001475568	8.19E-05	-2.75E-05	$1/(a + br + cr^2)$	3
6609.12	Fe I	6748.84	S I	5000-7000	6073.03	0.994752	-0.118793	$ab^{1/r}r^c$	2
6609.12	Fe I	6757.17	S I	4400-6900	5845.1056	1.0058528	-0.12878833	$ab^r r^c$	3
6680.15	Cr I	6703.57	Fe I	4800-6500	3635	2633	-967	130.6	$a + br + cr^2 + dr^3$	1
6703.57	Fe I	6721.85	Si I	4700-6550	6825.2988	-840.26077	-1038.0854	496.98698	$a + br + cr^2 + dr^3$	3
6710.31	Fe I	6713.76	Fe I	4800-6300	6674	-1353	233.29	$a + br + cr^2$	1
6710.31	Fe I	6721.85	Si I	3750-5700	6105.508	-1551.6196	691.66748	-176.15435	$a + br + cr^2 + dr^3$	3
6710.31	Fe I	6767.77	Ni I	3700-6000	6949	-10279.7	20503.9	-15335.9	$a + br + cr^2 + dr^3$	2
6717.69	Ca I	6757.17	S I	5300-6800	5926.58	1.17997	-0.138265	$ab^{1/r}r^c$	2
6717.69	Ca I	6757.17	S I	7200-7700	8158	-686.136	$a + br$	2
6721.85	Si I	6771.04	Co I	3750-6250	5554.4503	0.91377129	0.060535721	$ab^{1/r}r^c$	3
6721.85	Si I	6839.83	Fe I	4800-6400	3783.9506	1939.4483	-521.88679	49.382188	$a + br + cr^2 + dr^3$	3
6748.84	S I	6750.15	Fe I	4900-6800	6194.06	1.004298	0.138792	$ab^{1/r}r^c$	2
6748.84	S I	6767.77	Ni I	5000-6800	6307.54	1.005136	0.148183	$ab^{1/r}r^c$	2
6750.15	Fe I	6757.17	S I	4700-7000	6044.21	1.00735	-0.125622	$ab^{1/r}r^c$	2
6757.17	S I	6767.77	Ni I	4800-6700	6169.4	1.00416	0.145267	$ab^{1/r}r^c$	2
6806.85	Fe I	6848.57	Si I	4700-6700	7116	-790.9	$a + br$	1
7110.90	Ni I	7022.39	Fe I	5300-6500	6492	-791.06341	$a + b \log(r)$	3
7110.90	Ni I	7022.95	Fe I	3500-6600	7775	-5150.6755	325.81723	6084.4549	-4007.2797	...	$a + br + cr^2 + dr^3 + er^4$	3
7110.90	Ni I	7034.90	Si I	4500-6700	5677.678	0.9068567	-0.090936813	$ab^r r^c$	3
7110.90	Ni I	7071.88	Fe I	5050-6500	6066	-1076.6458	$a + b \log(r)$	3
7110.90	Ni I	7090.38	Fe I	3900-6500	6957	796.9239	-16020.09	25423.295	-12379.132	...	$a + br + cr^2 + dr^3 + er^4$	3
7110.90	Ni I	7130.92	Fe I	4300-7000	7740.5691	-8974.467	12385.913	-6956.3501	$a + br + cr^2 + dr^3$	3
7110.90	Ni I	7132.99	Fe I	5500-6050	5989.5842	748.53279	-1124.968	$a + br + cr^2$	3
7110.90	Ni I	7181.19	Fe I	4200-7000	7926.6838	-8555.0465	10974.93	-5542.4826	$a + br + cr^2 + dr^3$	3
7112.18	Fe I	7022.95	Fe I	4300-6000	7924.3779	-8118.8128	8946.0425	-4311.6523	$a + br + cr^2 + dr^3$	3
7112.18	Fe I	7034.90	Si I	3800-6700	7348.5613	-5185.4006	3691.6343	-967.50273	$a + br + cr^2 + dr^3$	3
7216.18	Ti I	7132.99	Fe I	3500-5900	6365.0976	-2170.5471	1242.9243	-491.89608	$a + br + cr^2 + dr^3$	3
7216.18	Ti I	7181.19	Fe I	3500-5800	6463.9587	-4488.1749	5325.8248	-2628.69	$a + br + cr^2 + dr^3$	3

continued on next page

Table 3. continued.

λ_1 [Å]	Ion	λ_2 [Å]	Ion	ΔT_{eff} [K]	a	b	c	d	e	f	Function	Ref.
7216.18	Ti I	7221.20	Fe I	3500-5800	6284.6629	-1527.7419	$a + br$	3
7251.71	Ti I	7142.52	Fe I	4200-6800	7654.0242	-3858.2697	2899.9181	-1135.2843	$a + br + cr^2 + dr^3$	3
7251.71	Ti I	7181.19	Fe I	4300-6900	5441.5977	-0.4745018	-0.39033324	$a(r - b)^c$	3
7327.65	Ni I	7375.25	Si I	3500-5250	5833.1952	-1992.5838	1774.5887	-857.75968	$a + br + cr^2 + dr^3$	3
7357.73	Ti I	7445.75	Fe I	4400-5400	5781.7635	-1570.4442	$a + br$	3
7461.52	Fe I	7491.65	Fe I	4400-5800	6414.7319	-1800.1392	$a + br$	3
7461.52	Fe I	7495.07	Fe I	4400-5800	6152.7548	-2318.461	$a + br$	3
7461.52	Fe I	7507.27	Fe I	4400-5900	7604.3548	-7135.3851	8481.292	-4440.1886	$a + br + cr^2 + dr^3$	3
7540.43	Fe I	7511.02	Fe I	4700-6000	6613.917	-14032.5	41178.67	-45064.2	$a + br + cr^2 + dr^3$	3
7540.43	Fe I	7563.01	Fe I	5000-6300	5198.713	-0.1799965	ar^b	3
7583.79	Fe I	7468.31	N I	5700-7000	7052.4777	-895.819	234.25416	-30.425818	1.4601492	...	$a + br + cr^2 + dr^3 + er^4$	3
7583.79	Fe I	7531.14	Fe I	3500-6600	5973.5196	3784.5656	-4235.942	$a + br + cr^2$	3
7583.79	Fe I	7586.02	Fe I	3500-6900	11021.68	-38217.372	138605.19	-248399.82	209495.81	-67865.923	$a + br + cr^2 + dr^3 + er^4 + fr^5$	3
7714.27	Ni I	7680.27	Si I	3500-6900	7193	-29.77509	-1681.5027	731.7729	-95.782326	...	$a + br + cr^2 + dr^3 + er^4$	3
7714.27	Ni I	7780.56	Fe I	5900-7000	9319.357	0.5872613	0.108473	$ab^r c^c$	3
7714.27	Ni I	7780.56	Fe I	3600-7000	7831.5986	-3202.7715	2050.2954	-1218.1437	$a + br + cr^2 + dr^3$	3
7723.21	Fe I	7680.27	Si I	3500-6000	7282.2329	-4432.9632	2956.9517	-776.4689	$a + br + cr^2 + dr^3$	3
7748.27	Fe I	7680.27	Si I	6500-7150	7979	-1601.28	$a + br$	3
7748.27	Fe I	7680.27	Si I	4600-7000	13167.773	-21440.335	27243.5	-15901.87	3287.8501	...	$a + br + cr^2 + dr^3 + er^4$	3
7748.27	Fe I	7832.20	Fe I	3500-6800	8443	-5245.24	6015.251	-4029.735	$a + br + cr^2 + dr^3$	3
7788.95	Ni I	7680.27	Si I	3500-7000	7554.168	-2001.119	252.7902	$a + br + cr^2$	3
7788.95	Ni I	7780.56	Fe I	3500-7000	7889.0498	-4728.7165	4151.1333	-2183.3018	$a + br + cr^2 + dr^3$	3
7788.95	Ni I	7832.20	Fe I	3500-7000	8477.5756	-7634.1137	8209.1666	-4105.5848	$a + br + cr^2 + dr^3$	3
7788.95	Ni I	7849.97	Si I	5200-7000	9151.883	-5400.7313	3647.6843	-991.87973	$a + br + cr^2 + dr^3$	3
7788.95	Ni I	7932.35	Si I	3500-7000	12176.034	-1.8245293	-0.73875711	$a(r - b)^c$	3
7788.95	Ni I	7944.00	Si I	4200-7000	11254.539	-30436.921	78629.353	-103193.97	64744.83	-15594.876	$a + br + cr^2 + dr^3 + er^4 + fr^5$	3
7912.87	Fe I	7680.27	Si I	5200-6800	7033.8179	-3523.7759	2431.6723	-589.24672	$a + br + cr^2 + dr^3$	3
7912.87	Fe I	7710.37	Fe I	5300-6800	7433.4687	-3131.7646	1119.1743	$a + br + cr^2$	3
8426.51	Ti I	7680.27	Si I	5300-6400	6963.6582	-2717.0084	967.28678	$a + br + cr^2$	3

Notes. From left to right, the first two columns give the wavelength of the line pairs adopted for the LDR, while column three gives the range in effective temperature in which the individual LDRs were calibrated. Columns four to nine list the coefficients of the analytical relation adopted for the calibration, while column ten gives the analytical formula. The last column gives the reference for the calibration of the LDR.

References. ⁽¹⁾ Kovtyukh & Gorlova (2000, KG); ⁽²⁾ Kovtyukh (2007, K07); ⁽³⁾ K17: this investigation.

Table 4. Atmospheric parameters, Fe abundances and radial velocities as a function of the pulsation phase for calibrating CCs.

Name	Dataset	MJD [d]	$T_{\text{eff}} \pm \sigma$ [K]	$\log g$	v_t [km s $^{-1}$]	$\text{Fe I} \pm \sigma$	$N_{\text{Fe I}}$	$\text{Fe II} \pm \sigma$	$N_{\text{Fe II}}$	$[\text{Fe}/\text{H}] \pm \sigma$	$RV \pm \sigma$ [km s $^{-1}$]
V340 Ara	FEROS	53620.0609687	5921 ± 154	2.0	4.9	0.29 ± 0.22	85	0.05 ± 0.13	4	0.11 ± 0.11	-76.9 ± 5.3
V340 Ara	UVES	54708.0671613	5181 ± 99	0.9	4.3	0.27 ± 0.20	86	0.24 ± 0.26	7	0.26 ± 0.16	-95.69 ± 0.03
V340 Ara	UVES	54709.0803304	5095 ± 99	0.7	4.8	0.21 ± 0.20	82	0.20 ± 0.26	6	0.21 ± 0.16	-91.37 ± 0.01
V340 Ara	UVES	56137.1372097	5172 ± 99	0.8	4.8	0.17 ± 0.15	93	0.18 ± 0.30	6	0.17 ± 0.14	-69.0 ± 0.2
V340 Ara	UVES	56138.0944950	5578 ± 119	0.9	4.9	0.26 ± 0.16	118	0.25 ± 0.06	8	0.25 ± 0.05	-73.2 ± 0.1
V340 Ara	UVES	56139.1860724	6083 ± 133	1.6	4.9	0.36 ± 0.16	104	0.33 ± 0.13	12	0.34 ± 0.10	-94.56 ± 0.06
V340 Ara	UVES	56152.0523667	4742 ± 108	1.1	4.8	0.11 ± 0.18	65	-0.18 ± 0.35	4	0.05 ± 0.16	-62.8 ± 0.2
eta Aql	STELLA	53935.9867868	5450 ± 97	0.9	3.4	0.20 ± 0.18	122	0.20 ± 0.04	7	0.20 ± 0.04	-15.4 ± 0.2
eta Aql	STELLA	53936.0890674	5469 ± 99	0.7	2.6	0.36 ± 0.14	102	0.37 ± 0.26	14	0.36 ± 0.12	-15.3 ± 0.2
eta Aql	STELLA	53944.0303995	5333 ± 99	1.2	4.2	0.15 ± 0.11	84	0.15 ± 0.14	10	0.15 ± 0.09	-9.3 ± 0.2
eta Aql	STELLA	53947.0833325	6116 ± 192	0.7	1.9	0.37 ± 0.20	98	0.37 ± 0.36	11	0.37 ± 0.18	-30.9 ± 0.2
eta Aql	STELLA	53949.0641156	5810 ± 161	0.8	2.4	0.48 ± 0.22	135	0.49 ± 0.14	9	0.49 ± 0.12	-21.6 ± 0.2
eta Aql	STELLA	53949.9577241	5617 ± 153	1.1	3.0	0.30 ± 0.18	121	0.31 ± 0.15	15	0.30 ± 0.12	-15.6 ± 0.2
eta Aql	STELLA	53950.9569429	5379 ± 100	1.2	4.4	0.16 ± 0.20	120	0.17 ± 0.28	13	0.16 ± 0.16	-12.2 ± 0.2
eta Aql	STELLA	53953.0029560	5659 ± 248	2.0	6.0	-0.03 ± 0.26	76	-0.03 ± 0.17	8	-0.03 ± 0.14	5.4 ± 0.2
eta Aql	STELLA	53958.9309528	5276 ± 138	0.7	2.4	0.36 ± 0.13	82	0.37 ± 0.11	10	0.36 ± 0.08	-1.6 ± 0.2
eta Aql	STELLA	53959.0331372	5311 ± 145	1.8	4.9	0.10 ± 0.21	115	0.10 ± 0.37	19	0.10 ± 0.18	-0.1 ± 0.2
eta Aql	STELLA	53962.0178211	5985 ± 238	1.1	2.5	0.39 ± 0.33	138	0.36 ± 0.38	15	0.37 ± 0.25	-30.0 ± 0.2
S Cru	HARPS	53150.1200407	6158 ± 182	1.7	2.9	0.19 ± 0.16	129	0.18 ± 0.19	16	0.19 ± 0.12	-8.8 ± 1.0
S Cru	HARPS	53151.0565227	6222 ± 61	1.7	3.0	0.12 ± 0.12	133	0.10 ± 0.12	18	0.11 ± 0.08	-18.9 ± 0.8
S Cru	HARPS	53152.1277898	5732 ± 63	1.2	2.3	0.16 ± 0.10	170	0.15 ± 0.15	18	0.15 ± 0.08	-7.7 ± 0.7
S Cru	HARPS	53153.0633060	5556 ± 100	1.4	3.0	0.01 ± 0.12	153	-0.03 ± 0.10	15	-0.01 ± 0.08	3.0 ± 0.8
S Cru	HARPS	53154.1283897	5612 ± 99	1.7	4.5	-0.03 ± 0.17	130	-0.04 ± 0.16	14	-0.03 ± 0.12	12.4 ± 1.2
S Cru	HARPS	53156.1212653	6013 ± 50	1.7	2.8	0.12 ± 0.12	152	0.14 ± 0.11	15	0.14 ± 0.08	-15.3 ± 0.7
S Cru	HARPS	53201.9852976	6482 ± 98	1.9	2.8	0.12 ± 0.12	122	0.08 ± 0.18	20	0.10 ± 0.10	-19.5 ± 1.0
S Cru	HARPS	53202.9803582	6058 ± 53	1.5	2.5	0.18 ± 0.11	146	0.17 ± 0.12	18	0.17 ± 0.08	-15.8 ± 0.7
S Cru	HARPS	53202.9856839	6051 ± 55	1.6	2.7	0.14 ± 0.10	145	0.17 ± 0.10	16	0.16 ± 0.07	-15.7 ± 0.7
S Cru	HARPS	53204.9630967	5517 ± 97	1.4	3.6	-0.03 ± 0.12	140	-0.01 ± 0.17	20	-0.03 ± 0.10	5.9 ± 0.9
S Cru	HARPS	53205.9747885	5784 ± 106	1.9	4.2	0.00 ± 0.12	120	-0.02 ± 0.13	15	-0.01 ± 0.09	11.5 ± 1.2
S Cru	HARPS	53206.9497352	6418 ± 98	1.7	2.7	0.09 ± 0.11	109	0.06 ± 0.21	21	0.08 ± 0.10	-21.1 ± 0.9
S Cru	FEROS	55284.3152681	6472 ± 93	1.9	3.1	-0.05 ± 0.19	94	-0.10 ± 0.28	12	-0.07 ± 0.16	-20.5 ± 1.0
beta Dor	HARPS	53015.1219391	5248 ± 93	1.5	3.9	-0.05 ± 0.14	165	-0.14 ± 0.11	13	-0.11 ± 0.09	14.0 ± 0.9
beta Dor	HARPS	53015.1239308	5236 ± 91	1.4	3.6	-0.05 ± 0.12	158	-0.10 ± 0.15	15	-0.07 ± 0.09	14.1 ± 0.9
beta Dor	HARPS	53015.1259288	5249 ± 90	1.5	3.9	-0.05 ± 0.13	159	-0.12 ± 0.14	16	-0.08 ± 0.09	14.1 ± 0.9
beta Dor	HARPS	53016.1700025	5195 ± 98	1.4	4.9	-0.10 ± 0.15	138	-0.07 ± 0.30	18	-0.10 ± 0.13	22.8 ± 1.2
beta Dor	HARPS	53016.1722763	5186 ± 98	1.4	4.9	-0.11 ± 0.15	137	-0.15 ± 0.20	14	-0.12 ± 0.12	22.8 ± 1.2
beta Dor	HARPS	53016.1745592	5203 ± 95	1.3	4.9	-0.13 ± 0.15	137	-0.08 ± 0.27	18	-0.12 ± 0.13	22.8 ± 1.2
beta Dor	HARPS	53017.1820488	5398 ± 160	1.1	3.7	-0.08 ± 0.12	108	-0.03 ± 0.11	12	-0.05 ± 0.08	26.2 ± 1.4
beta Dor	HARPS	53017.1844847	5392 ± 113	1.1	4.2	-0.11 ± 0.12	105	-0.06 ± 0.11	10	-0.08 ± 0.08	26.2 ± 1.4
beta Dor	HARPS	53017.1869331	5388 ± 139	1.1	4.9	-0.11 ± 0.13	106	-0.12 ± 0.21	12	-0.11 ± 0.11	26.2 ± 1.4
beta Dor	HARPS	53021.1802715	5992 ± 77	1.1	2.8	-0.01 ± 0.10	149	-0.03 ± 0.19	17	-0.01 ± 0.09	1.1 ± 0.7
beta Dor	HARPS	53021.1819217	5994 ± 90	1.3	3.3	0.01 ± 0.12	152	-0.04 ± 0.17	19	-0.01 ± 0.10	1.2 ± 0.7
beta Dor	HARPS	53021.1835549	6006 ± 75	1.2	3.0	0.03 ± 0.11	151	-0.03 ± 0.16	15	0.01 ± 0.09	1.2 ± 0.7
beta Dor	HARPS	53021.1852025	6001 ± 85	1.2	2.8	-0.01 ± 0.10	143	-0.03 ± 0.17	16	-0.01 ± 0.09	1.1 ± 0.7
beta Dor	HARPS	53023.1329203	5563 ± 73	1.5	3.7	-0.03 ± 0.13	164	-0.07 ± 0.15	17	-0.05 ± 0.10	-1.9 ± 0.7
beta Dor	HARPS	53023.1345710	5556 ± 71	1.3	3.2	-0.00 ± 0.12	162	0.01 ± 0.18	21	0.00 ± 0.10	-1.9 ± 0.7
beta Dor	HARPS	53023.1362075	5559 ± 82	1.5	3.7	-0.04 ± 0.13	160	-0.01 ± 0.19	20	-0.03 ± 0.11	-1.9 ± 0.7
beta Dor	HARPS	53023.1378355	5560 ± 69	1.4	3.4	-0.03 ± 0.12	168	-0.01 ± 0.17	20	-0.02 ± 0.10	-1.9 ± 0.7
beta Dor	HARPS	53025.1738720	5229 ± 93	1.3	3.6	-0.04 ± 0.13	158	-0.01 ± 0.25	20	-0.03 ± 0.11	15.9 ± 1.0
beta Dor	HARPS	53025.1759601	5229 ± 92	1.2	3.6	-0.03 ± 0.13	156	-0.04 ± 0.25	21	-0.03 ± 0.12	15.9 ± 1.0
beta Dor	HARPS	53025.1780493	5227 ± 90	1.2	3.5	-0.03 ± 0.14	160	-0.02 ± 0.26	21	-0.03 ± 0.12	16.0 ± 1.0
beta Dor	HARPS	53026.0920026	5207 ± 97	1.5	4.9	-0.12 ± 0.14	135	-0.09 ± 0.29	19	-0.12 ± 0.13	23.3 ± 1.2
beta Dor	HARPS	53026.0942576	5203 ± 99	1.4	4.9	-0.13 ± 0.15	135	-0.07 ± 0.23	17	-0.11 ± 0.13	23.3 ± 1.2
beta Dor	HARPS	53028.1694909	5692 ± 110	1.5	3.9	-0.05 ± 0.10	129	-0.03 ± 0.13	10	-0.04 ± 0.08	11.0 ± 0.9
beta Dor	HARPS	53028.1718352	5684 ± 129	1.5	3.8	-0.04 ± 0.09	126	-0.06 ± 0.17	13	-0.04 ± 0.08	10.9 ± 0.9
beta Dor	HARPS	53028.1741878	5689 ± 99	1.7	4.9	-0.10 ± 0.11	128	-0.06 ± 0.17	13	-0.09 ± 0.09	10.9 ± 0.9
beta Dor	HARPS	53029.1306027	5814 ± 90	1.4	3.3	-0.01 ± 0.10	148	0.01 ± 0.11	10	-0.00 ± 0.07	1.8 ± 0.8
beta Dor	HARPS	53029.1325697	5809 ± 83	1.3	3.4	-0.02 ± 0.11	151	0.01 ± 0.08	11	0.00 ± 0.06	1.8 ± 0.8
beta Dor	HARPS	53029.1339932	5810 ± 84	1.3	3.3	-0.01 ± 0.11	149	0.04 ± 0.06	10	0.03 ± 0.05	1.7 ± 0.8
beta Dor	HARPS	53029.1355791	5793 ± 86	1.4	3.5	-0.03 ± 0.11	154	0.00 ± 0.11	13	-0.02 ± 0.08	1.7 ± 0.8
beta Dor	HARPS	53031.1330521	5971 ± 89	1.3	3.0	0.01 ± 0.11	153	0.00 ± 0.15	13	0.00 ± 0.09	1.0 ± 0.7
beta Dor	HARPS	53031.1346849	5981 ± 80	1.3	3.0	0.00 ± 0.11	152	0.04 ± 0.07	11	0.03 ± 0.06	1.0 ± 0.7
beta Dor	HARPS	53031.1363173	5991 ± 85	1.2	2.9	0.06 ± 0.10	146	0.07 ± 0.08	10	0.07 ± 0.06	1.0 ± 0.7
beta Dor	HARPS	53032.1781164	5730 ± 73	1.6	3.7	-0.03 ± 0.12	150	-0.01 ± 0.16	18	-0.02 ± 0.10	-5.5 ± 0.8
beta Dor	HARPS	53032.1796472	5714 ± 81	1.3	3.4	-0.04 ± 0.12	152	-0.03 ± 0.11	16	-0.03 ± 0.08	-5.5 ± 0.8
beta Dor	HARPS	53032.1811734	5732 ± 75	1.6	3.8	-0.03 ± 0.12	154	-0.02 ± 0.16	17	-0.02 ± 0.10	-5.5 ± 0.8
beta Dor	HARPS	53033.1060160	5526 ± 74	1.4	3.2	0.01 ± 0.11	159	0.05 ± 0.18	21	0.02 ± 0.09	-1.2 ± 0.7
beta Dor	HARPS	53033.1077288	5531 ± 76	1.3	3.2	0.02 ± 0.11	165	0.01 ± 0.18	21	0.02 ± 0.10	-1.2 ± 0.7
beta Dor	HARPS	53033.1094348	5525 ± 78	1.3	3.3	-0.03 ± 0.12	159	0.00 ± 0.18	21	-0.02 ± 0.10	-1.2 ± 0.7
beta Dor	HARPS	53034.1394979	5340 ± 81	1.3	3.4	-0.01 ± 0.13	171	-0.10 ± 0.14	15	-0.05 ± 0.09	7.8 ± 0.9
beta Dor	HARPS	53034.142812	5331 ± 74	1.3	3.3	-0.03 ± 0.12	164	0.01 ± 0.22	21	-0.02 ± 0.10	7.8 ± 0.9
beta Dor	HARPS	53035.1331423	5227 ± 92	1.5	3.8	-0.03 ± 0.15	167	-0.09 ± 0.17	15	-0.06 ± 0.11	17.0 ± 1.0
beta Dor	HARPS	53035.1352292	5219 ± 86	1.4	4.1	-0.09 ± 0.14	158	-0.17 ± 0.15	15	-0.13 ± 0.10	17.0 ± 1.0
beta Dor	HARPS	53036.1369181	5210 ± 91	1.0	4.0	-0.12 ± 0.14	130	-0.08 ± 0.21	16	-0.11 ± 0.12	24.5 ± 1.2
beta Dor	HARPS	53036.1391838	5213 ± 96	1.3	4.9	-0.15 ± 0.15	132	-0.10 ± 0.27	15	-0.14 ± 0.13	24.5 ± 1.2
beta Dor	HARPS	53037.1									

Table 4. continued.

Name	Dataset	MJD [d]	$T_{\text{eff}} \pm \sigma$ [K]	$\log g$	v_t [km s $^{-1}$]	$\text{Fe I} \pm \sigma$	$N_{\text{Fe I}}$	$\text{Fe II} \pm \sigma$	$N_{\text{Fe II}}$	$[\text{Fe/H}] \pm \sigma$	$RV \pm \sigma$ [km s $^{-1}$]
zeta Gem	HARPS	53016.1805731	5216 ± 100	1.4	4.9	-0.02 ± 0.15	144	-0.01 ± 0.29	15	-0.02 ± 0.13	17.0 ± 1.0
zeta Gem	HARPS	53016.1829469	5216 ± 97	1.2	4.4	-0.02 ± 0.14	135	-0.02 ± 0.28	17	-0.02 ± 0.13	17.1 ± 1.0
zeta Gem	HARPS	53016.1853382	5213 ± 71	1.6	4.9	-0.04 ± 0.14	143	0.06 ± 0.30	17	-0.02 ± 0.13	17.1 ± 1.0
zeta Gem	HARPS	53017.1932375	5322 ± 96	1.2	4.9	-0.04 ± 0.14	121	-0.04 ± 0.24	12	-0.04 ± 0.12	20.2 ± 1.2
zeta Gem	HARPS	53017.1957591	5305 ± 92	1.1	4.9	-0.04 ± 0.13	112	-0.05 ± 0.21	13	-0.05 ± 0.11	20.2 ± 1.2
zeta Gem	HARPS	53017.1982693	5337 ± 100	1.3	4.9	0.01 ± 0.14	127	-0.01 ± 0.22	13	0.00 ± 0.12	20.2 ± 1.2
zeta Gem	HARPS	53021.1893175	5818 ± 64	1.1	3.0	0.10 ± 0.11	162	0.10 ± 0.13	12	0.10 ± 0.08	-0.1 ± 0.7
zeta Gem	HARPS	53021.1915396	5837 ± 60	1.2	3.1	0.15 ± 0.11	164	0.14 ± 0.12	11	0.14 ± 0.08	-0.1 ± 0.7
zeta Gem	HARPS	53021.1937450	5812 ± 80	1.1	3.0	0.13 ± 0.12	162	0.11 ± 0.15	13	0.12 ± 0.09	-0.1 ± 0.7
zeta Gem	HARPS	53021.1959571	5829 ± 61	1.3	2.8	0.14 ± 0.11	158	0.12 ± 0.21	14	0.13 ± 0.10	-0.1 ± 0.7
zeta Gem	HARPS	53021.1981818	5819 ± 59	1.2	3.0	0.14 ± 0.12	166	0.11 ± 0.17	13	0.13 ± 0.10	-0.1 ± 0.7
zeta Gem	HARPS	53023.1432110	5597 ± 86	1.4	3.3	0.11 ± 0.12	169	0.14 ± 0.18	18	0.12 ± 0.10	-4.7 ± 0.7
zeta Gem	HARPS	53023.1451185	5585 ± 93	1.5	3.7	0.05 ± 0.13	161	0.06 ± 0.18	17	0.05 ± 0.11	-4.7 ± 0.7
zeta Gem	HARPS	53023.1470277	5586 ± 74	1.4	3.5	0.06 ± 0.13	163	0.07 ± 0.19	17	0.06 ± 0.11	-4.7 ± 0.7
zeta Gem	HARPS	53023.1489287	5585 ± 63	1.5	3.6	0.05 ± 0.13	168	0.08 ± 0.19	18	0.06 ± 0.11	-4.6 ± 0.7
zeta Gem	HARPS	53025.1826223	5270 ± 74	1.1	3.2	0.07 ± 0.12	163	-0.01 ± 0.18	16	0.05 ± 0.10	9.0 ± 0.8
zeta Gem	HARPS	53025.1846603	5272 ± 74	1.3	3.4	0.04 ± 0.11	153	0.02 ± 0.20	17	0.03 ± 0.09	9.1 ± 0.8
zeta Gem	HARPS	53025.1867120	5276 ± 74	1.4	3.6	0.09 ± 0.12	156	0.00 ± 0.11	14	0.04 ± 0.08	9.1 ± 0.8
zeta Gem	HARPS	53026.0991063	5210 ± 83	1.3	3.6	0.03 ± 0.15	149	0.02 ± 0.27	19	0.03 ± 0.13	15.7 ± 1.0
zeta Gem	HARPS	53026.1014177	5200 ± 80	1.7	4.9	-0.04 ± 0.15	141	-0.06 ± 0.15	14	-0.05 ± 0.10	15.7 ± 1.0
zeta Gem	HARPS	53026.1030860	5209 ± 74	1.6	4.9	-0.03 ± 0.15	148	-0.08 ± 0.14	13	-0.06 ± 0.10	15.7 ± 1.0
zeta Gem	HARPS	53028.1798104	5503 ± 89	1.3	4.9	-0.00 ± 0.15	132	-0.03 ± 0.18	14	-0.01 ± 0.12	15.7 ± 1.1
zeta Gem	HARPS	53028.1825204	5505 ± 99	1.5	4.9	-0.02 ± 0.13	124	-0.09 ± 0.12	10	-0.06 ± 0.09	15.7 ± 1.1
zeta Gem	HARPS	53029.1395744	5617 ± 67	1.0	3.3	0.12 ± 0.12	143	0.10 ± 0.12	12	0.11 ± 0.09	5.8 ± 0.8
zeta Gem	HARPS	53029.1413379	5637 ± 76	1.4	4.1	0.11 ± 0.14	155	0.09 ± 0.18	15	0.10 ± 0.11	5.8 ± 0.8
zeta Gem	HARPS	53031.1410447	5813 ± 62	1.2	3.1	0.12 ± 0.12	168	0.10 ± 0.15	13	0.11 ± 0.09	0.1 ± 0.7
zeta Gem	HARPS	53031.1432571	5816 ± 93	1.3	3.1	0.12 ± 0.12	164	0.16 ± 0.13	12	0.14 ± 0.09	0.1 ± 0.7
zeta Gem	HARPS	53031.1454644	5814 ± 61	1.2	3.0	0.14 ± 0.12	165	0.15 ± 0.12	10	0.14 ± 0.08	0.1 ± 0.7
zeta Gem	HARPS	53032.2008798	5755 ± 99	1.2	3.1	0.15 ± 0.12	157	0.15 ± 0.07	11	0.15 ± 0.06	-3.6 ± 0.7
zeta Gem	HARPS	53032.2028918	5767 ± 62	1.4	3.0	0.13 ± 0.12	163	0.15 ± 0.15	12	0.14 ± 0.09	-3.7 ± 0.7
zeta Gem	HARPS	53032.2049165	5770 ± 67	1.2	3.0	0.13 ± 0.12	166	0.13 ± 0.12	11	0.13 ± 0.09	-3.7 ± 0.7
zeta Gem	HARPS	53033.1145522	5621 ± 65	1.3	3.2	0.06 ± 0.12	158	0.07 ± 0.18	18	0.06 ± 0.10	-5.2 ± 0.7
zeta Gem	HARPS	53033.1164296	5626 ± 72	1.4	3.4	0.12 ± 0.12	158	0.10 ± 0.19	16	0.11 ± 0.10	-5.2 ± 0.7
zeta Gem	HARPS	53033.1183039	5613 ± 77	1.5	3.7	-0.01 ± 0.13	164	-0.01 ± 0.18	16	-0.01 ± 0.10	-5.2 ± 0.7
zeta Gem	HARPS	53034.1506477	5422 ± 68	1.4	3.3	0.04 ± 0.13	178	-0.00 ± 0.09	14	0.01 ± 0.08	0.2 ± 0.7
zeta Gem	HARPS	53034.1525448	5429 ± 74	1.5	3.5	0.09 ± 0.13	176	0.01 ± 0.10	13	0.04 ± 0.08	0.3 ± 0.7
zeta Gem	HARPS	53034.1544641	5428 ± 71	1.2	3.0	0.13 ± 0.13	184	0.03 ± 0.11	14	0.07 ± 0.09	0.3 ± 0.7
zeta Gem	HARPS	53035.1428640	5288 ± 73	1.4	3.6	0.05 ± 0.11	168	-0.01 ± 0.15	16	0.03 ± 0.09	7.7 ± 0.8
zeta Gem	HARPS	53035.1443945	5289 ± 74	1.3	3.2	0.09 ± 0.12	172	0.05 ± 0.14	16	0.07 ± 0.09	7.7 ± 0.8
zeta Gem	HARPS	53035.1459297	5288 ± 73	1.2	3.1	0.10 ± 0.12	173	0.05 ± 0.15	16	0.08 ± 0.09	7.8 ± 0.8
zeta Gem	HARPS	53036.1547434	5222 ± 95	1.4	3.6	0.01 ± 0.14	152	-0.04 ± 0.14	14	-0.02 ± 0.10	15.1 ± 1.0
zeta Gem	HARPS	53036.1569325	5216 ± 86	1.1	3.3	0.06 ± 0.13	149	-0.03 ± 0.17	15	0.03 ± 0.10	15.1 ± 1.0
zeta Gem	HARPS	53037.1617356	5264 ± 95	1.3	4.9	-0.02 ± 0.16	128	0.01 ± 0.28	11	-0.01 ± 0.14	20.0 ± 1.2
zeta Gem	HARPS	53037.1642405	5247 ± 79	1.3	4.9	-0.03 ± 0.15	132	0.01 ± 0.24	15	-0.02 ± 0.13	20.0 ± 1.2
zeta Gem	STELLA	54348.2456000	5560 ± 114	0.9	2.4	0.32 ± 0.16	120	0.32 ± 0.24	13	0.32 ± 0.13	8.7 ± 0.2
zeta Gem	STELLA	54368.2539931	5529 ± 98	0.9	3.0	0.20 ± 0.17	114	0.23 ± 0.11	10	0.22 ± 0.09	11.9 ± 0.2
zeta Gem	STELLA	54373.2568361	5532 ± 99	1.0	2.4	0.26 ± 0.12	128	0.36 ± 0.15	13	0.30 ± 0.09	-2.6 ± 0.2
zeta Gem	STELLA	54417.2497900	5245 ± 90	0.8	4.4	0.11 ± 0.09	78	0.12 ± 0.27	10	0.11 ± 0.08	20.7 ± 0.2
zeta Gem	STELLA	54418.1548977	5427 ± 100	1.9	6.4	0.03 ± 0.11	91	0.03 ± 0.11	7	0.03 ± 0.08	20.3 ± 0.2
zeta Gem	STELLA	54418.1581293	5460 ± 117	1.8	4.7	0.12 ± 0.14	96	0.12 ± 0.06	6	0.12 ± 0.05	20.3 ± 0.2
zeta Gem	STELLA	54418.1730308	5404 ± 96	0.8	3.8	0.17 ± 0.12	96	0.03 ± 0.12	7	0.10 ± 0.08	20.2 ± 0.2
zeta Gem	STELLA	54421.2745932	5734 ± 140	0.8	2.5	0.29 ± 0.15	137	0.26 ± 0.16	13	0.28 ± 0.11	0.8 ± 0.2
zeta Gem	STELLA	54423.2824759	5606 ± 100	1.1	2.5	0.22 ± 0.12	129	0.23 ± 0.18	15	0.22 ± 0.10	-5.2 ± 0.2
zeta Gem	STELLA	54438.2882356	5339 ± 84	0.7	3.8	0.10 ± 0.16	123	0.13 ± 0.23	11	0.11 ± 0.13	21.5 ± 0.2
zeta Gem	STELLA	54462.2237082	5793 ± 92	0.8	2.2	0.32 ± 0.10	149	0.29 ± 0.17	13	0.31 ± 0.09	0.8 ± 0.2
zeta Gem	STELLA	54463.0747703	5762 ± 92	0.9	2.4	0.21 ± 0.10	144	0.22 ± 0.15	12	0.21 ± 0.08	-1.9 ± 0.2
zeta Gem	STELLA	54465.0558349	5455 ± 92	0.9	2.3	0.28 ± 0.12	158	0.30 ± 0.19	20	0.28 ± 0.10	0.5 ± 0.2
zeta Gem	STELLA	54471.1486908	5708 ± 94	1.0	2.4	0.23 ± 0.11	161	0.36 ± 0.16	11	0.28 ± 0.09	1.9 ± 0.2
zeta Gem	STELLA	54486.1579739	5341 ± 81	0.9	2.7	0.20 ± 0.13	161	0.16 ± 0.26	20	0.19 ± 0.12	6.4 ± 0.2
zeta Gem	STELLA	54501.1521642	5693 ± 94	0.6	2.5	0.28 ± 0.14	142	0.28 ± 0.10	10	0.28 ± 0.08	3.6 ± 0.2
zeta Gem	STELLA	54502.0078883	5742 ± 100	1.0	2.5	0.22 ± 0.11	149	0.29 ± 0.11	11	0.25 ± 0.08	1.2 ± 0.2
zeta Gem	STELLA	54525.0767616	5594 ± 97	0.8	2.8	0.18 ± 0.14	151	0.19 ± 0.04	10	0.19 ± 0.04	-4.5 ± 0.2
zeta Gem	STELLA	54557.9765317	5256 ± 98	0.8	2.6	0.20 ± 0.14	143	0.18 ± 0.38	21	0.20 ± 0.13	12.7 ± 0.2
zeta Gem	STELLA	54701.2370873	5239 ± 91	0.9	3.5	0.13 ± 0.14	124	0.17 ± 0.25	15	0.14 ± 0.12	20.2 ± 0.2
zeta Gem	STELLA	54702.2340611	5327 ± 97	0.8	3.7	0.09 ± 0.15	111	0.14 ± 0.17	12	0.11 ± 0.11	20.9 ± 0.2
zeta Gem	STELLA	54702.2373032	5380 ± 100	1.1	4.7	0.03 ± 0.13	110	0.00 ± 0.11	11	0.01 ± 0.08	20.9 ± 0.2
zeta Gem	STELLA	54703.2347503	5542 ± 107	1.0	2.9	0.15 ± 0.13	130	0.22 ± 0.12	11	0.19 ± 0.09	11.5 ± 0.2
zeta Gem	STELLA	54703.2379968	5522 ± 98	1.2	3.3	0.13 ± 0.12	123	0.15 ± 0.12	11	0.14 ± 0.08	11.4 ± 0.2
zeta Gem	STELLA	54704.2296119	5670 ± 93	1.0	2.9	0.16 ± 0.11	133	0.17 ± 0.17	12	0.16 ± 0.09	3.1 ± 0.2
zeta Gem	STELLA	54704.2378082	5673 ± 89	1.2	2.7	0.21 ± 0.14	156	0.24 ± 0.17	13	0.22 ± 0.11	3.1 ± 0.2
zeta Gem	STELLA	54705.2363817	5727 ± 87	1.2	2.4	0.20 ± 0.12	152	0.23 ± 0.18	12	0.21 ± 0.10	1.0 ± 0.2
zeta Gem	STELLA	54705.2396542	5734 ± 81	1.2	2.3	0.21 ± 0.13	168	0.25 ± 0.20	12	0.22 ± 0.11	1.0 ± 0.2
zeta Gem	STELLA	54706.2239765	5815 ± 100	0.8	2.4	0.19 ± 0.12	146	0.08 ± 0.17	11	0.15 ± 0.10	-0.3 ± 0.2
zeta Gem	STELLA	54706.2318500	5806 ± 97	0.9	2.3	0.21 ± 0.12	148	0.11 ± 0.19	13	0.18 ± 0.10	-0.3 ± 0.2
zeta Gem	STELLA	54706.2350952	5840 ± 99	1.0	2.3	0.28 ± 0.11	147	0.14 ± 0.23	13	0.25 ± 0.10	

Table 4. continued.

Name	Dataset	MJD [d]	$T_{\text{eff}} \pm \sigma$ [K]	$\log g$	v_t [km s $^{-1}$]	$\text{Fe I} \pm \sigma$	$N_{\text{Fe I}}$	$\text{Fe II} \pm \sigma$	$N_{\text{Fe II}}$	$[\text{Fe/H}] \pm \sigma$	$RV \pm \sigma$ [km s $^{-1}$]
zeta Gem	STELLA	54709.2409483	5371 ± 78	1.0	2.3	0.21 ± 0.12	156	0.23 ± 0.22	18	0.21 ± 0.11	4.8 ± 0.2
zeta Gem	STELLA	54711.2070298	5209 ± 99	0.8	3.5	0.08 ± 0.12	125	0.15 ± 0.24	14	0.09 ± 0.11	19.2 ± 0.2
zeta Gem	STELLA	54711.2102754	5239 ± 94	0.7	3.4	0.12 ± 0.12	131	0.14 ± 0.20	13	0.12 ± 0.10	19.2 ± 0.2
zeta Gem	STELLA	54712.2037665	5334 ± 87	1.2	4.4	0.03 ± 0.13	116	0.08 ± 0.16	12	0.05 ± 0.10	21.4 ± 0.2
zeta Gem	STELLA	54712.2070077	5327 ± 89	1.1	5.0	-0.04 ± 0.13	114	-0.03 ± 0.16	12	-0.03 ± 0.10	21.4 ± 0.2
zeta Gem	STELLA	54712.2427809	5331 ± 90	1.2	4.0	0.03 ± 0.15	133	0.08 ± 0.15	12	0.05 ± 0.11	21.4 ± 0.2
zeta Gem	STELLA	54713.2441852	5540 ± 93	0.9	2.9	0.18 ± 0.10	118	0.22 ± 0.20	10	0.19 ± 0.09	13.1 ± 0.2
zeta Gem	STELLA	54714.1983269	5647 ± 100	1.1	2.8	0.18 ± 0.10	118	0.23 ± 0.14	10	0.20 ± 0.08	4.1 ± 0.2
zeta Gem	STELLA	54714.2015666	5639 ± 99	1.3	2.7	0.17 ± 0.13	136	0.42 ± 0.10	8	0.34 ± 0.08	4.1 ± 0.2
zeta Gem	STELLA	54714.2418747	5658 ± 100	1.1	3.0	0.16 ± 0.13	145	0.12 ± 0.15	11	0.14 ± 0.10	3.8 ± 0.2
zeta Gem	STELLA	54729.1622480	5421 ± 98	1.2	2.6	0.19 ± 0.10	150	0.21 ± 0.17	13	0.19 ± 0.09	1.8 ± 0.2
zeta Gem	STELLA	54750.2108478	5304 ± 84	1.2	2.9	0.12 ± 0.09	139	0.17 ± 0.15	15	0.13 ± 0.08	7.8 ± 0.2
zeta Gem	STELLA	54754.2167227	5614 ± 99	1.2	3.1	0.15 ± 0.12	136	0.17 ± 0.18	12	0.16 ± 0.10	8.8 ± 0.2
zeta Gem	STELLA	54754.2210371	5594 ± 99	1.1	2.5	0.19 ± 0.12	131	0.25 ± 0.26	13	0.20 ± 0.11	8.8 ± 0.2
zeta Gem	STELLA	54760.1902531	5331 ± 83	1.2	2.4	0.23 ± 0.10	156	0.19 ± 0.04	9	0.20 ± 0.04	6.5 ± 0.2
zeta Gem	STELLA	54760.1934999	5337 ± 91	0.7	2.3	0.26 ± 0.12	157	0.20 ± 0.20	17	0.24 ± 0.10	6.5 ± 0.2
zeta Gem	STELLA	54760.1972571	5343 ± 80	1.1	2.8	0.14 ± 0.11	158	0.14 ± 0.12	13	0.14 ± 0.08	6.5 ± 0.2
zeta Gem	STELLA	54760.2005072	5331 ± 84	1.1	2.6	0.18 ± 0.10	150	0.21 ± 0.18	18	0.19 ± 0.09	6.6 ± 0.2
zeta Gem	STELLA	54760.2037406	5335 ± 96	1.1	2.6	0.20 ± 0.12	160	0.18 ± 0.23	18	0.19 ± 0.10	6.6 ± 0.2
zeta Gem	STELLA	54760.2069893	5335 ± 81	1.0	2.6	0.17 ± 0.11	155	0.13 ± 0.17	14	0.16 ± 0.09	6.6 ± 0.2
zeta Gem	STELLA	54760.2260601	5334 ± 79	1.1	2.7	0.17 ± 0.11	161	0.13 ± 0.07	11	0.15 ± 0.06	6.7 ± 0.2
zeta Gem	STELLA	54760.2292960	5346 ± 76	1.1	2.5	0.21 ± 0.11	153	0.24 ± 0.21	16	0.21 ± 0.10	6.8 ± 0.2
zeta Gem	STELLA	54760.2489259	5333 ± 80	1.3	2.6	0.19 ± 0.12	165	0.24 ± 0.12	13	0.22 ± 0.09	7.0 ± 0.2
zeta Gem	STELLA	54760.2521595	5328 ± 79	0.8	2.5	0.19 ± 0.11	156	0.14 ± 0.27	17	0.18 ± 0.10	7.0 ± 0.2
zeta Gem	STELLA	54760.2554083	5321 ± 77	1.0	2.8	0.16 ± 0.11	155	0.18 ± 0.19	17	0.17 ± 0.10	7.0 ± 0.2
zeta Gem	STELLA	54762.2238400	5219 ± 93	0.8	3.6	0.13 ± 0.17	130	0.14 ± 0.22	14	0.13 ± 0.13	20.3 ± 0.2
zeta Gem	STELLA	54777.0470244	5800 ± 99	0.7	2.0	0.34 ± 0.12	152	0.27 ± 0.24	13	0.32 ± 0.11	0.1 ± 0.2
zeta Gem	STELLA	54789.0010630	5613 ± 81	0.8	2.5	0.21 ± 0.11	157	0.28 ± 0.07	12	0.26 ± 0.06	-4.5 ± 0.2
zeta Gem	STELLA	54789.0043057	5626 ± 96	0.6	2.6	0.22 ± 0.09	146	0.19 ± 0.01	7	0.19 ± 0.01	-4.5 ± 0.2
zeta Gem	STELLA	54789.0128166	5609 ± 87	0.8	2.4	0.29 ± 0.10	134	0.25 ± 0.14	16	0.28 ± 0.08	-4.4 ± 0.2
zeta Gem	STELLA	54789.0160527	5618 ± 94	0.8	2.5	0.22 ± 0.09	132	0.20 ± 0.14	16	0.21 ± 0.08	-4.4 ± 0.2
zeta Gem	STELLA	54789.0192991	5605 ± 90	0.9	2.5	0.20 ± 0.08	130	0.23 ± 0.11	15	0.21 ± 0.06	-4.4 ± 0.2
zeta Gem	STELLA	54792.9898339	5241 ± 91	0.7	3.2	0.13 ± 0.09	107	0.12 ± 0.05	9	0.12 ± 0.04	21.3 ± 0.2
zeta Gem	STELLA	54792.9930840	5270 ± 85	0.9	3.9	0.07 ± 0.14	120	0.08 ± 0.17	15	0.08 ± 0.11	21.3 ± 0.2
zeta Gem	STELLA	54793.0106374	5270 ± 87	0.8	3.7	0.07 ± 0.07	87	0.08 ± 0.22	16	0.07 ± 0.06	21.4 ± 0.2
zeta Gem	STELLA	54793.9876861	5470 ± 96	1.2	4.4	0.04 ± 0.09	86	0.05 ± 0.18	12	0.04 ± 0.08	17.9 ± 0.2
zeta Gem	STELLA	54793.9912187	5466 ± 99	1.3	3.9	0.09 ± 0.12	110	0.10 ± 0.16	13	0.09 ± 0.10	17.8 ± 0.2
zeta Gem	STELLA	54794.9869237	5603 ± 74	1.1	3.2	0.14 ± 0.12	132	0.15 ± 0.13	13	0.14 ± 0.09	7.3 ± 0.2
zeta Gem	STELLA	54797.9939915	5797 ± 89	1.1	2.5	0.31 ± 0.10	136	0.30 ± 0.22	15	0.31 ± 0.09	-2.2 ± 0.2
zeta Gem	STELLA	54798.9745787	5624 ± 93	0.8	2.5	0.31 ± 0.11	150	0.30 ± 0.16	15	0.30 ± 0.09	-4.8 ± 0.2
zeta Gem	STELLA	54798.9778207	5632 ± 97	0.4	2.0	0.38 ± 0.10	120	0.39 ± 0.13	11	0.39 ± 0.08	-4.8 ± 0.2
zeta Gem	STELLA	54799.9715934	5466 ± 99	1.1	2.7	0.19 ± 0.11	159	0.19 ± 0.14	18	0.19 ± 0.08	0.3 ± 0.2
zeta Gem	STELLA	54799.9748388	5486 ± 90	1.0	2.5	0.23 ± 0.07	129	0.23 ± 0.19	20	0.23 ± 0.07	0.3 ± 0.2
zeta Gem	STELLA	54800.9882545	5300 ± 87	0.8	2.6	0.23 ± 0.10	145	0.24 ± 0.24	18	0.23 ± 0.09	8.2 ± 0.2
zeta Gem	STELLA	54822.2375649	5241 ± 80	1.1	3.4	0.13 ± 0.13	152	0.14 ± 0.32	18	0.13 ± 0.12	15.3 ± 0.2
Y Oph	HARPS	53150.2730135	5540 ± 96	1.1	3.1	0.00 ± 0.14	176	0.04 ± 0.27	14	0.01 ± 0.12	-4.5 ± 0.7
Y Oph	HARPS	53152.2897868	5564 ± 100	1.4	3.9	-0.00 ± 0.14	165	0.02 ± 0.20	11	0.00 ± 0.12	-0.1 ± 0.8
Y Oph	HARPS	53154.2444076	5628 ± 94	1.3	3.6	0.01 ± 0.15	157	0.05 ± 0.16	12	0.03 ± 0.11	1.1 ± 0.8
Y Oph	HARPS	53156.2027098	5758 ± 91	1.1	3.6	0.09 ± 0.15	165	0.15 ± 0.12	11	0.13 ± 0.09	-2.7 ± 0.7
Y Oph	HARPS	53201.1235014	5562 ± 99	0.8	2.9	0.13 ± 0.15	176	0.17 ± 0.19	14	0.14 ± 0.12	-5.8 ± 0.7
Y Oph	HARPS	53203.1387889	5524 ± 75	1.1	3.2	-0.03 ± 0.13	166	-0.01 ± 0.27	14	-0.02 ± 0.12	-1.0 ± 0.8
Y Oph	HARPS	53216.2394193	5707 ± 106	0.6	2.8	0.14 ± 0.13	185	0.09 ± 0.20	14	0.13 ± 0.11	-11.2 ± 0.6
Y Oph	HARPS	56213.9822101	5663 ± 99	0.5	2.7	0.14 ± 0.13	180	0.09 ± 0.17	12	0.13 ± 0.11	-9.6 ± 0.6
RS Pup	HARPS	53048.1059728	5083 ± 103	0.4	4.9	-0.00 ± 0.19	72	-0.01 ± 0.23	7	-0.00 ± 0.15	44.6 ± 2.0
RS Pup	HARPS	53052.1267735	6238 ± 132	2.0	4.9	0.02 ± 0.17	82	-0.07 ± 0.28	15	-0.00 ± 0.14	17.1 ± 2.3
RS Pup	HARPS	53054.1528518	6184 ± 135	1.0	3.6	0.17 ± 0.11	104	0.24 ± 0.29	10	0.18 ± 0.10	4.9 ± 1.3
RS Pup	HARPS	53056.1793367	6037 ± 121	0.8	3.7	0.21 ± 0.11	109	0.23 ± 0.19	8	0.22 ± 0.10	3.1 ± 1.1
RS Pup	HARPS	53058.1901193	5769 ± 133	0.8	4.9	0.14 ± 0.14	120	0.11 ± 0.27	10	0.14 ± 0.13	4.3 ± 1.0
RS Pup	HARPS	53060.1785463	5593 ± 100	0.6	4.9	0.14 ± 0.13	129	0.17 ± 0.04	5	0.17 ± 0.04	6.5 ± 0.9
RS Pup	HARPS	53062.1660897	5438 ± 98	0.5	4.9	0.16 ± 0.15	130	0.14 ± 0.09	9	0.14 ± 0.07	9.3 ± 0.9
RS Pup	HARPS	53064.1739999	5346 ± 99	0.6	4.9	0.14 ± 0.14	128	0.11 ± 0.22	12	0.13 ± 0.12	12.2 ± 0.9
RS Pup	HARPS	53066.1524561	5266 ± 97	0.7	4.9	0.10 ± 0.15	142	0.12 ± 0.27	12	0.11 ± 0.13	15.3 ± 1.0
RS Pup	HARPS	53149.9663503	5206 ± 100	0.6	4.9	0.10 ± 0.13	132	0.06 ± 0.25	10	0.09 ± 0.12	16.1 ± 1.0
RS Pup	HARPS	53151.9756287	5171 ± 82	0.8	4.9	0.08 ± 0.15	138	0.01 ± 0.19	10	0.05 ± 0.12	19.2 ± 1.1
RS Pup	HARPS	53153.9783769	5135 ± 99	1.0	4.0	0.14 ± 0.11	126	0.10 ± 0.15	8	0.12 ± 0.09	22.3 ± 1.1
RS Pup	HARPS	53155.9674458	5089 ± 90	1.0	4.9	0.13 ± 0.14	131	0.17 ± 0.28	13	0.14 ± 0.13	25.4 ± 1.2
RS Pup	HARPS	53155.9756820	5085 ± 95	0.9	4.9	0.11 ± 0.13	123	0.13 ± 0.24	10	0.11 ± 0.11	25.4 ± 1.2
UZ Set	FEROS	54190.3602653	4824 ± 121	1.3	4.9	0.14 ± 0.28	69	0.28 ± 0.44	9	0.18 ± 0.24	52.3 ± 1.8
UZ Set	FEROS	54190.3817051	4822 ± 99	1.3	4.9	0.02 ± 0.26	70	0.13 ± 0.41	9	0.05 ± 0.22	52.4 ± 1.9
UZ Set	UVES	54906.4044778	5382 ± 100	1.1	4.9	0.19 ± 0.19	102	0.14 ± 0.21	9	0.17 ± 0.14	19.37 ± 0.01
UZ Set	UVES	54923.3689441	5088 ± 99	1.6	4.8	0.14 ± 0.19	90	0.02 ± 0.17	7	0.07 ± 0.13	30.95 ± 0.01
UZ Set	UVES	56137.1617631	4797 ± 98	0.9	4.8	0.11 ± 0.17	71	-0.01 ± 0.19	7	0.06 ± 0.13	59.6 ± 0.1
UZ Set	UVES	56152.0662646	4769 ± 98	0.9	4.8	-0.01 ± 0.22	78	-0.19 ± 0.33	10	-0.07 ± 0.18	60.5 ± 0.1
UZ Set	UVES	56160.1647217	5295 ± 99	1.3	4.9	0.16 ± 0.15	127	0.17 ± 0.28	15	0.16 ± 0.13	19.77 ± 0.04
UZ Set	UVES	56175.0512628	5275 ± 99	1.5	4.9	0.18 ± 0.15	120	0.20 ± 0.29	16	0.18 ± 0.13	

Table 4. continued.

Name	Dataset	MJD [d]	$T_{\text{eff}} \pm \sigma$ [K]	$\log g$	v_t [km s $^{-1}$]	$\text{Fe I} \pm \sigma$	$N_{\text{Fe I}}$	$\text{Fe II} \pm \sigma$	$N_{\text{Fe II}}$	$[\text{Fe/H}] \pm \sigma$	$RV \pm \sigma$ [km s $^{-1}$]
AV Sgr	UVES	56136.2000040	5051 ± 100	1.3	4.8	0.20 ± 0.15	104	0.18 ± 0.11	7	0.19 ± 0.09	22.5 ± 0.1
AV Sgr	UVES	56152.0841941	4999 ± 97	1.3	4.8	0.20 ± 0.18	111	0.10 ± 0.30	9	0.18 ± 0.15	25.0 ± 0.1
AV Sgr	UVES	56168.0466724	4991 ± 99	1.6	4.8	0.25 ± 0.18	106	0.16 ± 0.34	9	0.23 ± 0.16	28.8 ± 0.1
VY Sgr	FEROS	53522.2280817	6136 ± 150	1.6	5.0	0.41 ± 0.30	100	0.33 ± 0.05	5	0.33 ± 0.05	-7.8 ± 1.5
VY Sgr	FEROS	53550.1640986	5678 ± 146	1.0	4.9	0.33 ± 0.33	73	0.27 ± 0.14	6	0.28 ± 0.13	-11.5 ± 1.2
VY Sgr	FEROS	53551.2196741	5388 ± 122	0.8	4.9	0.33 ± 0.27	75	0.21 ± 0.16	5	0.25 ± 0.14	-5.8 ± 0.9
VY Sgr	FEROS	53616.0926172	6269 ± 149	1.9	5.0	0.40 ± 0.31	77	0.43 ± 0.22	5	0.42 ± 0.18	9.5 ± 0.9
VY Sgr	FEROS	54189.2893288	5317 ± 118	0.9	4.9	0.24 ± 0.25	118	0.30 ± 0.15	4	0.29 ± 0.13	0.1 ± 0.8
VY Sgr	FEROS	54189.3107431	5269 ± 99	0.8	3.9	0.21 ± 0.19	114	0.26 ± 0.29	5	0.23 ± 0.16	0.3 ± 0.8
VY Sgr	UVES	54923.3591348	5107 ± 112	1.3	3.8	0.22 ± 0.16	86	0.29 ± 0.33	10	0.23 ± 0.14	16.44 ± 0.02
VY Sgr	UVES	56160.1810996	4882 ± 86	0.3	4.8	0.07 ± 0.18	79	0.11 ± 0.23	5	0.09 ± 0.14	38.7 ± 0.1
VY Sgr	UVES	56162.1638617	5202 ± 97	0.3	4.9	0.10 ± 0.17	69	0.12 ± 0.08	6	0.12 ± 0.07	45.6 ± 0.1
VY Sgr	UVES	56168.0638766	5419 ± 99	0.9	3.8	0.21 ± 0.15	127	0.28 ± 0.17	11	0.25 ± 0.11	-4.59 ± 0.05
XX Sgr	UVES	54599.4044771	6313 ± 167	1.8	3.5	0.01 ± 0.14	82	-0.07 ± 0.15	15	-0.03 ± 0.10	6.01 ± 0.04
XX Sgr	UVES	56054.2339884	5867 ± 91	1.3	2.6	0.15 ± 0.12	157	0.08 ± 0.14	17	0.12 ± 0.09	11.48 ± 0.02
XX Sgr	UVES	56136.2215481	6259 ± 76	1.1	2.3	0.10 ± 0.11	118	0.07 ± 0.15	20	0.09 ± 0.09	0.91 ± 0.05
XX Sgr	UVES	56152.0466585	5511 ± 86	1.2	3.0	0.13 ± 0.14	139	0.07 ± 0.11	15	0.10 ± 0.08	21.53 ± 0.01
XX Sgr	UVES	56159.1275487	5465 ± 90	1.1	3.5	0.02 ± 0.16	131	-0.07 ± 0.15	20	-0.03 ± 0.11	29.60 ± 0.01
Y Sgr	HARPS	53149.2916913	5405 ± 91	1.2	4.1	-0.04 ± 0.16	102	-0.05 ± 0.21	13	-0.05 ± 0.13	8.1 ± 1.3
Y Sgr	HARPS	53149.2960838	5447 ± 99	1.3	4.9	-0.04 ± 0.17	100	-0.03 ± 0.20	10	-0.04 ± 0.13	8.1 ± 1.3
Y Sgr	HARPS	53150.2840780	5672 ± 120	2.0	4.9	-0.00 ± 0.14	70	0.02 ± 0.18	10	0.01 ± 0.11	17.8 ± 1.9
Y Sgr	HARPS	53150.2888491	5602 ± 193	1.8	4.9	-0.04 ± 0.14	78	-0.06 ± 0.02	5	-0.06 ± 0.02	17.8 ± 1.9
Y Sgr	HARPS	53151.2398841	6239 ± 145	2.0	3.4	0.11 ± 0.13	100	0.11 ± 0.07	13	0.11 ± 0.06	-15.3 ± 1.3
Y Sgr	HARPS	53151.2439506	6339 ± 100	2.0	3.1	0.18 ± 0.10	86	0.14 ± 0.08	13	0.16 ± 0.06	-15.4 ± 1.3
Y Sgr	HARPS	53152.2965307	6049 ± 131	2.0	4.4	0.04 ± 0.17	122	0.02 ± 0.14	14	0.03 ± 0.11	-15.6 ± 1.0
Y Sgr	HARPS	53152.2992080	6036 ± 104	2.0	4.2	0.01 ± 0.14	119	-0.01 ± 0.14	15	-0.00 ± 0.10	-15.5 ± 1.0
Y Sgr	HARPS	53156.3224439	5891 ± 208	1.9	4.9	0.06 ± 0.14	75	0.07 ± 0.23	9	0.06 ± 0.12	14.2 ± 1.9
Y Sgr	HARPS	53156.3273170	5906 ± 201	2.0	3.7	0.12 ± 0.11	74	0.10 ± 0.11	9	0.11 ± 0.08	14.0 ± 1.9
Y Sgr	HARPS	53202.1441349	5616 ± 164	1.8	4.9	-0.02 ± 0.13	77	-0.03 ± 0.15	11	-0.03 ± 0.10	17.5 ± 1.8
Y Sgr	HARPS	53202.1489274	5613 ± 125	1.6	4.4	-0.03 ± 0.11	74	-0.05 ± 0.11	8	-0.04 ± 0.08	17.5 ± 1.8
Y Sgr	HARPS	53203.1454884	6305 ± 99	2.0	3.3	0.16 ± 0.11	96	0.18 ± 0.11	13	0.17 ± 0.08	-13.9 ± 1.3
Y Sgr	HARPS	53203.1495670	6249 ± 106	2.0	3.7	0.11 ± 0.12	98	0.11 ± 0.09	12	0.11 ± 0.07	-14.0 ± 1.3
Y Sgr	HARPS	53204.1180208	6132 ± 140	2.0	4.9	-0.03 ± 0.17	102	-0.10 ± 0.17	15	-0.06 ± 0.12	-16.6 ± 1.1
Y Sgr	HARPS	53204.1206929	6112 ± 99	1.9	4.1	0.15 ± 0.16	110	0.08 ± 0.15	16	0.11 ± 0.11	-16.6 ± 1.1
Y Sgr	HARPS	53205.1591202	5728 ± 87	2.0	4.9	0.02 ± 0.16	133	-0.07 ± 0.23	16	-0.01 ± 0.13	-8.2 ± 1.0
Y Sgr	STELLA	54249.1753617	5826 ± 274	0.6	1.9	0.34 ± 0.26	114	0.34 ± 0.20	12	0.34 ± 0.16	-15.8 ± 0.2
Y Sgr	STELLA	54266.1156498	5962 ± 287	0.7	1.8	0.30 ± 0.20	82	0.31 ± 0.34	15	0.30 ± 0.17	-18.0 ± 0.2
Y Sgr	STELLA	54271.1069764	6182 ± 161	1.9	4.1	0.17 ± 0.20	82	0.15 ± 0.23	14	0.16 ± 0.15	-11.5 ± 0.2
Y Sgr	HARPS	56212.9902382	5734 ± 98	1.9	4.9	-0.05 ± 0.17	126	-0.05 ± 0.25	17	-0.05 ± 0.14	-9.5 ± 0.9
Y Sgr	HARPS	56240.0036931	6249 ± 97	2.0	5.0	0.07 ± 0.17	108	0.04 ± 0.16	14	0.06 ± 0.11	-15.3 ± 1.3
R TrA	HARPS	53150.1353086	5934 ± 143	2.0	4.9	0.04 ± 0.13	93	-0.18 ± 0.11	10	-0.09 ± 0.08	2.6 ± 1.4
R TrA	HARPS	53150.1453265	5910 ± 143	2.0	4.9	-0.01 ± 0.13	89	-0.18 ± 0.11	13	-0.11 ± 0.08	2.4 ± 1.4
R TrA	HARPS	53152.1394611	5814 ± 94	1.9	3.4	-0.01 ± 0.13	136	-0.03 ± 0.08	15	-0.02 ± 0.07	-11.6 ± 0.9
R TrA	HARPS	53152.1469512	5824 ± 95	1.8	3.2	0.04 ± 0.12	139	0.04 ± 0.09	17	0.04 ± 0.07	-11.4 ± 0.9
R TrA	HARPS	53154.1400956	6467 ± 84	2.0	3.7	0.02 ± 0.13	101	-0.09 ± 0.10	17	-0.05 ± 0.08	-22.7 ± 1.3
R TrA	HARPS	53154.1496573	6452 ± 96	2.0	2.9	0.07 ± 0.10	96	0.02 ± 0.10	14	0.04 ± 0.07	-23.0 ± 1.3
R TrA	HARPS	53156.1326474	5698 ± 102	2.0	4.9	-0.08 ± 0.12	104	-0.07 ± 0.14	15	-0.08 ± 0.09	-1.6 ± 1.1
R TrA	HARPS	53156.1414131	5745 ± 96	2.0	4.8	-0.02 ± 0.13	106	-0.03 ± 0.19	17	-0.03 ± 0.11	-1.5 ± 1.1
R TrA	HARPS	53201.0286305	5966 ± 109	2.0	4.3	0.03 ± 0.11	89	-0.03 ± 0.09	11	-0.01 ± 0.07	1.7 ± 1.3
R TrA	HARPS	53202.0246343	6277 ± 80	2.0	3.5	0.03 ± 0.11	96	-0.05 ± 0.14	18	-0.00 ± 0.08	-25.6 ± 1.2
R TrA	HARPS	53203.0415339	5799 ± 100	2.0	3.5	0.01 ± 0.13	133	0.00 ± 0.07	14	0.00 ± 0.06	-10.5 ± 0.9
R TrA	HARPS	53204.0101104	5836 ± 97	2.0	4.9	0.04 ± 0.11	96	-0.10 ± 0.18	14	-0.00 ± 0.09	3.0 ± 1.3
R TrA	HARPS	53205.0362291	6450 ± 98	2.0	3.5	0.01 ± 0.10	98	-0.06 ± 0.16	20	-0.01 ± 0.09	-24.1 ± 1.3
R TrA	HARPS	53206.0233396	5941 ± 79	1.8	2.8	0.12 ± 0.11	129	0.10 ± 0.14	15	0.12 ± 0.09	-17.5 ± 0.9
R TrA	FEROS	55283.3432676	6096 ± 90	2.0	4.9	-0.04 ± 0.21	86	-0.22 ± 0.20	11	-0.13 ± 0.14	-22.0 ± 1.1
RZ Vel	HARPS	53149.9869296	5321 ± 97	0.7	3.3	0.13 ± 0.10	150	0.04 ± 0.14	9	0.10 ± 0.08	16.7 ± 0.9
RZ Vel	HARPS	53151.9991635	5163 ± 97	1.2	4.1	0.07 ± 0.12	152	0.05 ± 0.07	7	0.05 ± 0.06	25.1 ± 1.1
RZ Vel	HARPS	53153.9963816	5041 ± 78	1.3	4.9	0.06 ± 0.14	125	0.02 ± 0.19	10	0.04 ± 0.11	33.5 ± 1.3
RZ Vel	HARPS	53155.9860314	4981 ± 85	1.6	4.9	0.02 ± 0.20	103	-0.13 ± 0.25	7	-0.04 ± 0.16	41.9 ± 1.8
RZ Vel	HARPS	53200.9387705	5409 ± 106	1.0	4.9	0.12 ± 0.14	77	0.05 ± 0.23	10	0.10 ± 0.12	41.3 ± 1.8
RZ Vel	HARPS	53201.9423125	5422 ± 100	0.9	4.9	0.08 ± 0.16	121	0.07 ± 0.13	9	0.08 ± 0.10	36.7 ± 1.4
RZ Vel	HARPS	53202.9406629	6245 ± 98	1.2	3.8	0.11 ± 0.10	102	0.10 ± 0.11	12	0.10 ± 0.07	29.6 ± 1.4
RZ Vel	HARPS	53203.9388780	6314 ± 192	1.2	5.0	0.06 ± 0.20	99	0.07 ± 0.15	9	0.06 ± 0.12	13.9 ± 1.2
RZ Vel	HARPS	53204.9383376	6474 ± 120	1.4	4.9	0.02 ± 0.15	101	0.04 ± 0.10	10	0.03 ± 0.08	0.6 ± 1.2
RZ Vel	HARPS	53205.9402008	6225 ± 100	1.5	4.9	0.14 ± 0.14	93	0.16 ± 0.08	8	0.16 ± 0.07	-2.6 ± 1.1
RZ Vel	FEROS	55280.0861358	5199 ± 99	1.2	4.9	-0.05 ± 0.28	93	0.08 ± 0.17	6	0.04 ± 0.15	49.1 ± 2.3
RZ Vel	HARPS	56606.1850289	5308 ± 110	1.6	4.9	0.18 ± 0.20	54	0.16 ± 0.27	5	0.18 ± 0.16	47.9 ± 2.6

Notes. The first three columns give the name of the target, the spectroscopic dataset, and the Modified Julian Date at which the spectrum was collected. Columns 4, 5, and 6 give the effective temperature and its standard deviation, the surface gravity, and the microturbulent velocity. The columns 7–8 and 9–10 list both Fe I and Fe II abundances and their standard deviations together with the number of lines adopted for the measurements. Column eleven gives the weighted mean of Fe I and Fe II abundances (weighted by $1/\sigma^2$) with its intrinsic error, while the last column gives the radial-velocity measurement and the respective uncertainty.

Table 5. High resolution spectra only adopted for radial-velocity measurements.

Name	Dataset	MJD [d]	$RV \pm \sigma$ [km s $^{-1}$]
V340 Ara	FEROS	53520.2213553	-99.7 ± 7.5
V340 Ara	FEROS	53521.2126174	-96.7 ± 5.8
V340 Ara	FEROS	53522.2102258	-93.9 ± 0.8
V340 Ara	FEROS	53523.2653732	-89.8 ± 0.7
V340 Ara	FEROS	53524.1628015	-85.8 ± 0.8
V340 Ara	FEROS	53549.3036618	-63.6 ± 14.4
V340 Ara	FEROS	53550.1532155	-64.6 ± 0.6
V340 Ara	FEROS	53551.1938192	-60.0 ± 0.6
V340 Ara	FEROS	53551.2732169	-59.1 ± 0.5
V340 Ara	FEROS	53552.3038235	-55.0 ± 0.8
V340 Ara	FEROS	53556.3161638	-65.7 ± 1.2
V340 Ara	FEROS	53556.3192516	-65.9 ± 1.4
V340 Ara	FEROS	53597.0374439	-63.3 ± 1.5
V340 Ara	FEROS	53599.0975102	-73.3 ± 5.2
V340 Ara	FEROS	53601.1158191	-93.3 ± 17.8
V340 Ara	FEROS	53602.1093876	-98.8 ± 13.7
V340 Ara	FEROS	53603.1099409	-100.2 ± 7.6
V340 Ara	FEROS	53609.0378955	-80.0 ± 0.5
V340 Ara	FEROS	53609.0424397	-80.0 ± 0.5
V340 Ara	FEROS	53615.0266904	-54.1 ± 0.8
V340 Ara	FEROS	53616.0536654	-51.5 ± 1.0
V340 Ara	FEROS	53617.0696186	-55.9 ± 1.3
V340 Ara	FEROS	53618.0534958	-64.5 ± 1.3
V340 Ara	FEROS	53619.0473470	-67.9 ± 1.0
V340 Ara	FEROS	53621.1257226	-81.0 ± 17.6
RS Pup	HARPS	53051.1389691	33.0 ± 4.4
UZ Sct	FEROS	53520.2424019	16.3 ± 1.0
UZ Sct	FEROS	53521.2331590	21.1 ± 0.9
UZ Sct	FEROS	53522.2357550	26.9 ± 1.0
UZ Sct	FEROS	53523.2847746	33.3 ± 1.1
UZ Sct	FEROS	53524.1926044	39.3 ± 1.0
UZ Sct	FEROS	53549.3253449	16.3 ± 1.1
UZ Sct	FEROS	53550.1730666	18.3 ± 1.0
UZ Sct	FEROS	53551.2382008	24.2 ± 1.0
UZ Sct	FEROS	53551.2431731	24.1 ± 1.0
UZ Sct	FEROS	53551.2475029	24.4 ± 1.0
UZ Sct	FEROS	53551.2518292	24.4 ± 0.9
UZ Sct	FEROS	53552.3179119	30.9 ± 1.0
UZ Sct	FEROS	53556.3564325	53.8 ± 1.6
UZ Sct	FEROS	53556.3615687	54.1 ± 1.3
UZ Sct	FEROS	53577.2848080	26.4 ± 1.0
UZ Sct	FEROS	53602.1340975	59.5 ± 2.2
UZ Sct	FEROS	53603.1347598	60.2 ± 2.1
UZ Sct	FEROS	53609.0764160	18.2 ± 0.8
UZ Sct	FEROS	53609.0815589	17.7 ± 0.9
UZ Sct	FEROS	53615.0471044	51.5 ± 1.6
UZ Sct	FEROS	53616.1000454	56.4 ± 2.0
UZ Sct	FEROS	53617.1424676	60.6 ± 2.2
UZ Sct	FEROS	53618.1711558	58.5 ± 2.1
UZ Sct	FEROS	53619.1658348	48.0 ± 1.3
UZ Sct	FEROS	53620.1685455	41.8 ± 1.3
UZ Sct	FEROS	53621.0360640	34.0 ± 0.9
AV Sgr	FEROS	53520.2272967	42.6 ± 2.0
AV Sgr	FEROS	53521.2192697	45.1 ± 2.4
AV Sgr	FEROS	53522.2164015	34.9 ± 1.4
AV Sgr	FEROS	53523.2705083	21.9 ± 1.2
AV Sgr	FEROS	53524.1671280	16.9 ± 1.2
AV Sgr	FEROS	53550.1575431	39.0 ± 1.6
AV Sgr	FEROS	53551.1663433	43.5 ± 1.4
AV Sgr	FEROS	53551.1768545	43.2 ± 2.0
AV Sgr	FEROS	53551.2794534	43.0 ± 2.3
AV Sgr	FEROS	53552.3294632	44.3 ± 2.8
AV Sgr	FEROS	53556.3258803	-2.0 ± 1.2
AV Sgr	FEROS	53556.3363054	-1.3 ± 1.2
AV Sgr	FEROS	53577.2606543	17.5 ± 1.0
AV Sgr	FEROS	53597.0421718	42.0 ± 1.9
AV Sgr	FEROS	53599.1027847	36.9 ± 1.6
AV Sgr	FEROS	53603.1196862	-7.9 ± 1.5
AV Sgr	FEROS	53609.0474987	24.0 ± 1.1
AV Sgr	FEROS	53609.0537392	23.0 ± 1.3
AV Sgr	FEROS	53615.0318342	28.6 ± 1.4
AV Sgr	FEROS	53616.0863475	22.1 ± 1.1
AV Sgr	FEROS	53617.1247625	11.1 ± 1.3
AV Sgr	FEROS	53618.1537678	3.5 ± 2.2
AV Sgr	FEROS	53619.1482114	-7.9 ± 1.3
AV Sgr	FEROS	53620.1526565	-3.7 ± 1.1
VY Sgr	FEROS	53520.2344426	17.0 ± 0.9
VY Sgr	FEROS	53521.2256094	9.0 ± 1.1
VY Sgr	FEROS	53523.2768347	-10.6 ± 1.1
VY Sgr	FEROS	53524.1851391	-4.8 ± 0.9

continued on next page

Table 5. continued.

Name	Dataset	MJD [d]	$RV \pm \sigma$ [km s $^{-1}$]
VY Sgr	FEROS	53549.3172633	-7.4 ± 1.7
VY Sgr	FEROS	53551.2057981	-5.7 ± 0.9
VY Sgr	FEROS	53551.2141933	-5.7 ± 0.9
VY Sgr	FEROS	53551.2252183	-5.9 ± 1.0
VY Sgr	FEROS	53552.3099053	2.6 ± 0.7
VY Sgr	FEROS	53556.3425215	32.3 ± 1.1
VY Sgr	FEROS	53556.3485575	32.2 ± 1.5
VY Sgr	FEROS	53577.2677235	-10.9 ± 1.4
VY Sgr	FEROS	53597.0481329	30.8 ± 1.6
VY Sgr	FEROS	53599.1090806	39.3 ± 2.5
VY Sgr	FEROS	53601.1784165	18.9 ± 1.0
VY Sgr	FEROS	53602.1267713	14.0 ± 0.9
VY Sgr	FEROS	53603.1265701	3.5 ± 1.0
VY Sgr	FEROS	53609.0614284	21.0 ± 1.0
VY Sgr	FEROS	53615.0381043	16.7 ± 1.0
VY Sgr	FEROS	53617.1312705	-7.3 ± 1.7
VY Sgr	FEROS	53618.1641875	-10.4 ± 1.3
VY Sgr	FEROS	53619.1559350	-4.5 ± 0.9
VY Sgr	FEROS	53620.1598186	3.1 ± 0.9
Y Sgr	HARPS	56553.1423824	-13.4 ± 1.0

Notes. From left to right the columns give the name of the target, the spectroscopic dataset, the Modified Julian Date, and the radial-velocity measurements together with their standard deviations.